

AN ABSTRACT OF THE THESIS OF

Shou-Kong Lancelot Wang for the degree of Master of Science  
in Nuclear Engineering presented on June 3, 1980

Title: High Speed Motion Neutron Radiography of Two-Phase  
Flow

Abstract Approved: \_\_\_\_\_

~~Redacted for Privacy~~

Alan H. Robinson

Current research in the area of two-phase flow utilizes a wide variety of sensing devices, but some limitations exist on the information which can be obtained. Neutron radiography is a feasible alternative to "see" the two-phase flow. A system to perform neutron radiographic analysis of dynamic events which occur on the order of several milliseconds has been developed at Oregon State University. Two different methods have been used to radiograph the simulated two-phase flow. These pulsed or "flash" radiography and high speed movie neutron radiography serve as a "snapshot" with an exposure time ranging from 10 to 20 milliseconds. In high speed movie radiography, a scintillator is used to convert neutrons into light which is enhanced by an optical intensifier and then photographed by a high speed camera.

Both types of radiography utilize the pulsing capability of the OSU TRIGA reactor. In order to predict the visibility of the images in two-phase flow, two computer codes, an  $S_N$  program and a Monte Carlo program, have been written.

The visibility is expressed in the relative neutron density on the film. The principle difficulty with this type of neutron radiography is the fogging of the image due to the large amount of scattering in the water. This difficulty can be overcome by using thin regions for the two-phase flow, heavy water instead of light water, or an anti-scatter grid. The improvement using an anti-scatter grid has been modeled with the computer programs.

The results obtained in this thesis demonstrate the feasibility of using neutron radiography to obtain data in two-phase flow situations. Both movies and flash radiographs have been obtained of air bubbles in water and boiling from a heater element. The neutron radiographs of the boiling element show both nucleate boiling and film boiling.

HIGH SPEED MOTION NEUTRON RADIOGRAPHY  
OF TWO-PHASE FLOW

by

Shou-Kong Lancelot Wang

A THESIS

submitted to

Oregon State University

in partial fulfillment of  
the requirements for the  
degree of

Master of Science

Commencement June 1981

APPROVED:

Redacted for Privacy

---

Professor of Nuclear Engineering

Redacted for Privacy

---

Head of Department of Nuclear Engineering

Redacted for Privacy

---

Dean of Graduate School

Date thesis is presented June 3, 1980

Typed by Mary Bauman for Shou-Kong Lancelot Wang

## ACKNOWLEDGEMENT

I would like to express thanks and appreciation to Dr. Alan Robinson, my major professor, from whom I received the major part of my nuclear engineering instruction. I am very grateful for the opportunity to have studied under him. Also my special thanks to Dr. C. H. Wang, chairman of the Department of Nuclear Engineering, for his guidance in every way and to his staff, in particular Terry Anderson and Bill Carpenter of Reactor Operations, for their willing assistance. I am also grateful to Dennis Tollefson, Y. C. Gao and Paul Schofield, my partners, for their assistance all the years long.

I dedicate this thesis to my parents.

Thank you, Lord.

## TABLE OF CONTENTS

<u>Chapter</u>	<u>Page</u>
I. Introduction . . . . .	1
1.1 Principles of Neutron Radiography . . . . .	1
1.2 Special Characteristics of Neutron Radiography . . . . .	3
1.3 Applications and Advantages of Neutron Radiography of Two-Phase Flow . . . . .	6
1.4 Scope of the Radiography of Two-Phase Flow . . . . .	9
II. Reactor Facilities . . . . .	11
2.1 Descriptions of OSTR . . . . .	11
2.2 Beam Port #3 Facility . . . . .	14
2.3 Thermal Neutron Flux Measurement . . . . .	20
2.4 OSTR Pulse Characteristics . . . . .	22
III. High Speed Motion Neutron Radiography . . . . .	27
3.1 System Design . . . . .	27
3.2 Neutron Scintillator Screen . . . . .	27
3.3 Image Intensifier . . . . .	29
3.4 High Speed Camera and Film . . . . .	30
3.5 Electronic Synchronization System . . . . .	30
3.6 Anti-Scatter Grid . . . . .	32
IV. Integrated Flux Pulsed Radiography . . . . .	35
4.1 System Design . . . . .	35
4.2 Gadolinium Foil and X-Ray Film . . . . .	35
V. Computer Modelings of the Scattering System . . . . .	38
5.1 $S_N$ Approximation Method . . . . .	38
5.2 Monte Carlo Method . . . . .	43
VI. Results and Conclusions . . . . .	50
6.1 Results . . . . .	50
6.2 Conclusions . . . . .	69
VII. Bibliography and Appendices . . . . .	71
Bibliography . . . . .	71
Appendix I - $S_N$ Approximation Code . . . . .	73
Appendix II - Monte Carlo Code . . . . .	78

## LIST OF ILLUSTRATIONS

<u>Figure</u>	<u>Page</u>
1.1 Schematic Drawing of the Equipment for Neutron Radiography	2
1.2 Thermal Neutron and X-Ray Total Mass Attenuation Coefficients of the Elements	5
2.1 Cutaway View of TRIGA Reactor	12
2.2 Cutaway View of TRIGA Reactor Core Arrangement	13
2.3 Horizontal Section of TRIGA Reactor	15
2.4 Beam Port #3 Facility	16
2.5 Shutter #1 and Collimators	17
2.6 Graph of NaI Efficiency Versus Energy	21
3.1 High Speed Motion Neutron Radiography System	28
3.2 Synchronization System	31
3.3 Anti-Scatter Grid	34
4.1 Integrated Flux Neutron Radiography System	37
5.1 Geometry of $S_N$ Approximation	42
5.2 Geometry of Monte Carlo Method	44
5.3 Flux Density Contours for BP #3 at Object Position	46
5.4 Diagram of Anisotropic Scattering	47
6.1 Steel Boxes	51
6.2 Air Bubble Pump and Heating Element	51
6.3 Integrated Flux Pulsed Radiography, $H_2O$ with Air Bubbles in Thick Box	54

<u>Figure</u>		<u>Page</u>
6.4	Integrated Flux Pulsed Radiography, H <sub>2</sub> O Boiling in Thick Box	54
6.5	Integrated Flux Pulsed Radiography, H <sub>2</sub> O with Air Bubbles in Thin Box	55
6.6	Integrated Flux Pulsed Radiography, H <sub>2</sub> O with Air Bubbles in Thin Box	55
6.7	Integrated Flux Pulsed Radiography, H <sub>2</sub> O with Air Bubbles in Thin Box	56
6.8	Integrated Flux Pulsed Radiography, H <sub>2</sub> O Boiling in Thin Box (Beginning of Boiling)	56
6.9	Integrated Flux Pulsed Radiography, H <sub>2</sub> O Boiling in Thin Box	57
6.10	Integrated Flux Pulsed Radiography, D <sub>2</sub> O with Air Bubbles in Thick Box	57
6.11	Integrated Flux Pulsed Radiography, D <sub>2</sub> O Boiling in Thick Box	58
6.12	Integrated Flux Pulsed Radiography, D <sub>2</sub> O with Air Bubbles in Thin Box	58
6.13	Integrated Flux Pulsed Radiography, D <sub>2</sub> O Boiling in Thin Box	59
6.14	Motion Radiography, Water with Air Bubble in Thin Box	60
6.15	Motion Radiography, Boiling Water in Thin Box	60
6.16	Motion Radiography, Boiling Water in Thin Box	61
6.17	Motion Radiography, Boiling Water in Thin Box	61
6.18	Motion Radiography, Boiling Water in Thin Box	62
6.19	Motion Radiography, Boiling Water in Thin Box	62

<u>Figure</u>		<u>Page</u>
6.20	Water with Air Bubbles with Exposure Time of 1 ms	64
6.21	Boiling Water with Exposure Time of 1 ms	64
6.22	Water with Air Bubbles with Exposure Time of 8 ms	65
6.23	Boiling Water with Exposure Time of 8 ms	65
6.24	Expected Visibility of a 0.5 cm - Diameter Bubble vs. Thickness of H <sub>2</sub> O Calculated by S <sub>N</sub> Approximation	67
6.25	Expected Visibility of a 0.5 cm - Diameter Bubble vs. Thickness of D <sub>2</sub> O Calculated by S <sub>N</sub> Approximation	67
6.26	Expected Visibility of a 0.5 cm - Diameter Bubble vs. Thickness of H <sub>2</sub> O Calculated by Monte Carlo Method	68
6.27	Expected Visibility of a 0.5 cm - Diameter Bubble vs. Thickness of D <sub>2</sub> O Calculated by Monte Carlo Method	68

## LIST OF TABLES

<u>Table</u>		<u>Page</u>
1.1	Total Microscopic Cross-Sections of Some Materials at Various Energies of Interest in Neutron Radiography	7
2.1	TRIGA Pulse Data	26
6.1	Expected and Measured Visibilities of a Bubble in Light and Heavy Water	66

# HIGH SPEED MOTION NEUTRON RADIOGRAPHY OF TWO-PHASE FLOW

## I. INTRODUCTION

### 1.1 Principles of Neutron Radiography

Neutron radiography uses neutrons to produce an image of certain materials intermixed with other materials. The main idea of neutron radiography is that the various elements with corresponding neutron cross-sections and physical shapes will exhibit different neutron penetrating capabilities which result in different responses on the film. For example, elements such as H, Li, B, Cd and many of the rare earths attenuate neutrons and can be "seen". Many materials, such as Pb, Bi, U and steel, only interact slightly with neutrons and can be "seen through". This difference allows examination of hydrogen-containing fluids, propellents and plastics, even when contained in heavy metals (1). This is the fundamental principle upon which neutron radiography of two-phase flow is based.

The schematic drawing of radiography system is shown in Figure 1.1. Assume that the combination of source and collimator provides  $I_0$  neutrons  $\text{cm}^{-2}\text{sec}^{-1}$  approximately normal to the face of the sample which has two components of lengths  $X$  and  $\Delta X$  and with effective attenuation coefficients  $\Sigma_1$ ,  $\Sigma_2$ .

From this simplified model, the uncollided neutron

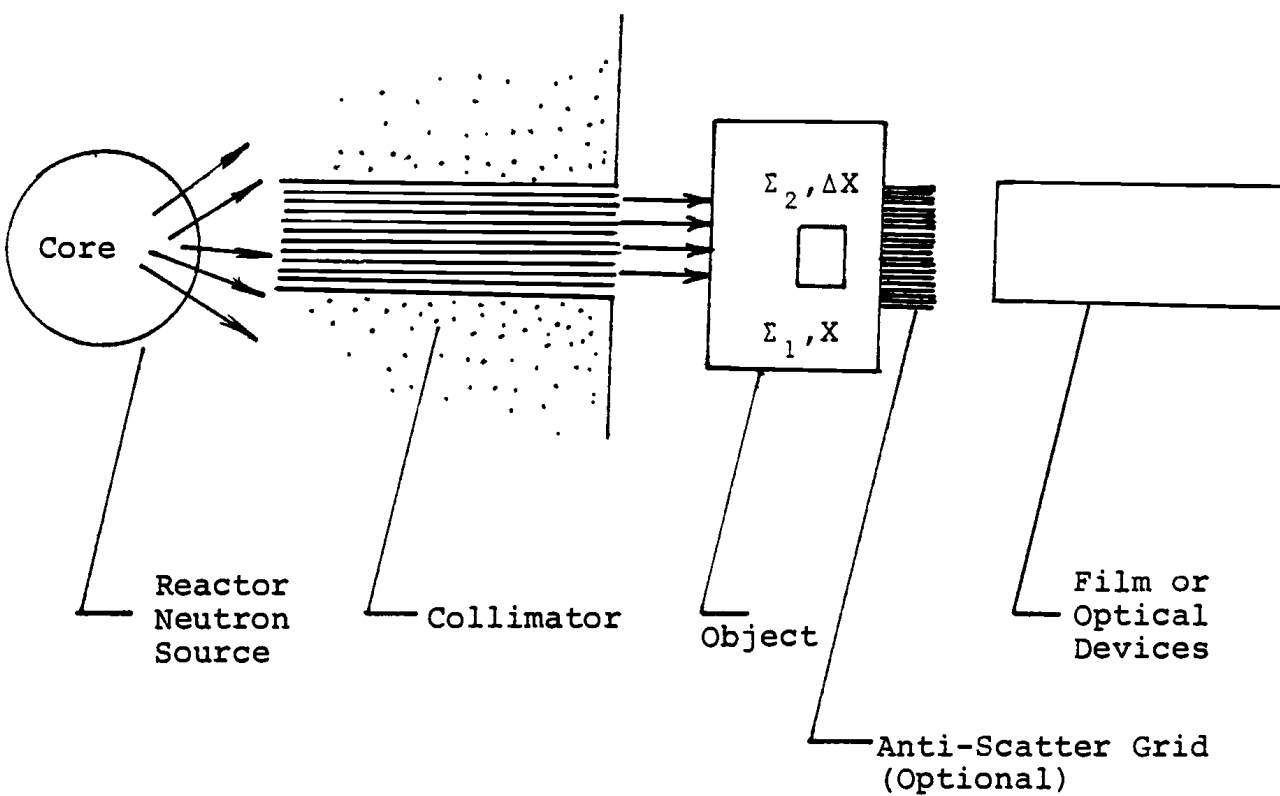


Figure 1.1 Schematic Drawing of the Equipment for Neutron Radiography

beam intensity from the two parts of the sample would be

$$I_1 = I_0 e^{-X} \quad (1-1)$$

$$I_2 = I_0 e^{-(\Sigma_1 (X-\Delta X) + \Sigma_2 \Delta X)} \quad (1-2)$$

In order to record the presence of the object in the target, for example, a bubble in water, the neutron intensity  $I_2$  would have to be adequate to affect the detector and the difference between  $I_1$  and  $I_2$  would have to be detectable. This simple model neglects the possible scatterings in the target (e.g., water) then causing responses on the image of the object (e.g., bubble) in the detector. A small collimator (here it is also called an anti-scatter grid) between the sample and the detector can reduce this effect. The anti-scatter grid is explained in detail in Chapter III.

## 1.2 Special Characteristics of Neutron Radiography

Neutrons are uncharged and their interaction with matter is therefore only through nuclear forces; this is the main distinction between neutron radiography and the well-developed X-radiography. It is well known that X-radiation is electromagnetic radiation of short wave length, with the result that an incoming X-ray interacts with the electron cloud around the nucleus. Since the electron cloud density increases with atomic number, the interaction between X-ray and electron cloud becomes stronger as atomic number

increases. Neutrons, on the other hand, are uncharged, so that a neutron has a high penetrating ability. But some elements are exceptions to this rule. These elements will be imaged readily and will also obviously be the essential materials in neutron radiography detector, such as Li, B, Cd and Gd, etc. However, the neutron mass attenuation coefficients of the elements present a "random" picture when plotted vs. atomic number. The X-ray mass attenuation coefficients, on the other hand, increase in a regular fashion. This comparison is shown in Figure 1.2. (2).

The fundamental consequences of the neutron interactions and their role on radiographic applications are:

1. The cross-section can vary markedly from nuclide to nuclide so it is possible to distinguish not only between materials with similar atomic number but also between isotopes. For example, natural uranium (mainly  $^{238}\text{U}$ ) can be distinguished from high neutron absorption cross-section isotope  $^{235}\text{U}$  in the reactor fuel element (3). Another striking application is that radiographs can be obtained of very light elements with high attenuation coefficients behind considerable thickness of heavy elements with low attenuation coefficients. In the radiography of two-phase flow, the combination is water and steel. Hydrogenous materials such as water or plastics give high scattering of

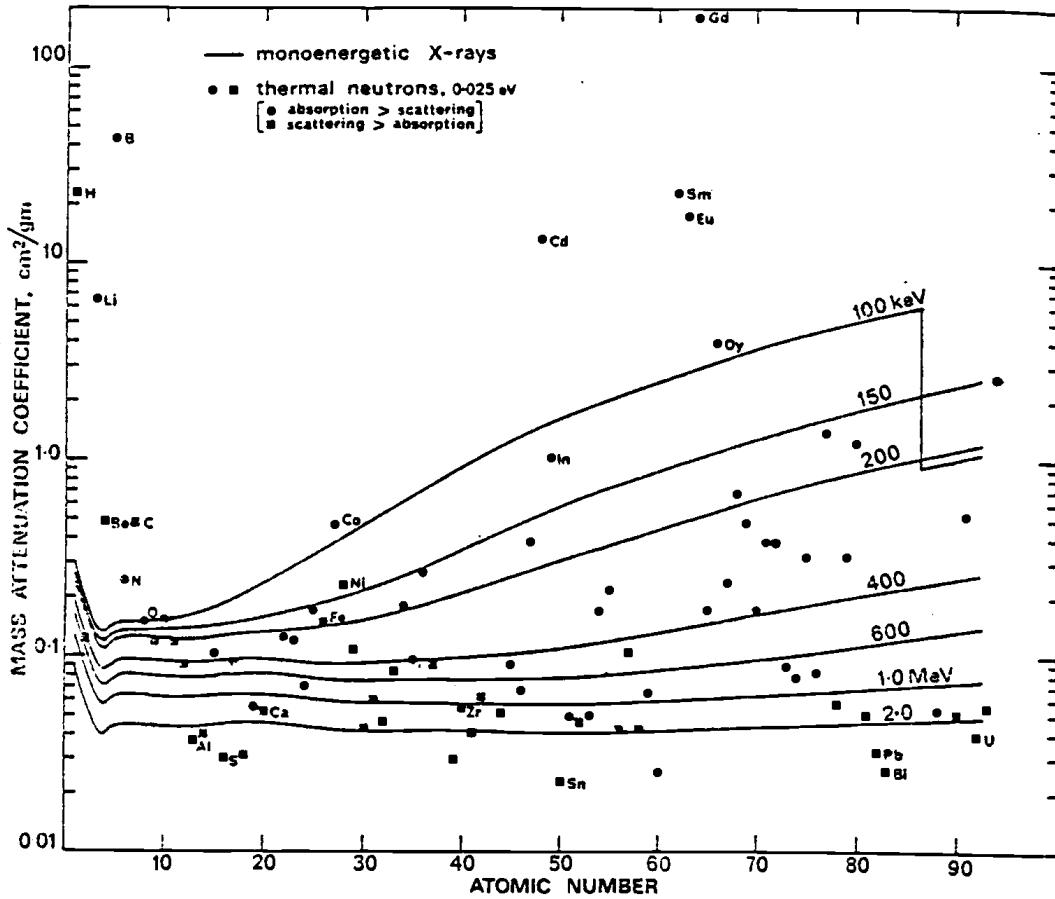


Figure 1.2 Thermal Neutron (0.025) and X-Ray Total Mass Attenuation Coefficients of the Elements.

neutrons because the scattering cross-section of hydrogen is very high. This cross-section is even increased by a factor of four when the hydrogen atom is bound in a heavy molecule (4). Other examples are boron, lithium and, at higher masses, cadmium and gadolinium can be easily detected even when covered by heavy elements. Boric acid streams in a steel chamber have been radiographed successfully at Oregon State University (5).

2. The cross-section of a nuclide for neutrons can vary markedly from one energy to another because of resonances in the neutron-nucleus interaction. The reason that most neutron radiographies utilize thermal neutrons is because most materials have  $1/v$  ( $v$  = neutron velocity) response to an incident neutron beam, so that there is little contrast between materials for fast neutrons compared with the large resonances in the thermal range. This phenomenon is shown in Table 1.1 (6).

### 1.3 Applications and Advantages of Neutron Radiography of Two-Phase Flow

Current research in the area of two-phase flow utilizes a wide variety of sensing devices. Measurements are made of temporal and spatial variations in velocity and pressure fields in each phase. While measurements can be made to a

Table 1.1 Total Microscopic Cross-Sections  
of Some Materials at Various Energies  
of Interest in Neutron Radiography

Material	0.025 eV	Resonances (Energy in Brackets)		2.6 MeV	10 MeV	14 MeV
Water	103	None		42	41	41
Lithium	72	11 (260 keV)		1.9	1.6	1.4
Aluminium	1.6	53 (5.9 keV)	35 (35 keV)	3.2	1.7	1.7
Iron	14	6,700 (1.1 keV)	85 (26 keV)	3.3	3.1	2.6
Cadmium	2,475	7,800 (0.175 eV)	130 (28 eV)	4.8	4.5	4.5
Indium	193	29,000 (1.45 eV)	900 (3.9 eV)	5.0	4.5	4.5
Gadolinium	50,000	310 (2.05 eV)	1300 (2.6 eV)	6.5	5.1	5.2
Lead	11	10.7 (350 keV)	8.1 (520 keV)	7.0	5.1	5.3
Dysprosium	1,057	1,050 (1.75 eV)	7,400 (5.5 eV)	6.6	5.2	5.2
Uranium	16	4,200 (6.6 eV)	2,200 (21 eV)	7.6	5.6	5.7

higher degree of accuracy, but some limitations exist on the information which can be obtained. For example, the probes can disturb the flow fields making the results dependent on the method of measurement. For studies of rod bundles, measurements must transverse to the flow channels and transparent flow channels are usually used which constrain the system pressures.

When the neutron radiographic technique is applied, the forementioned limitations can be overcome. Several potential advantages might be realized

1. Neutron radiography is non-destructive. The neutron flux won't disturb the flow fields and physical properties even in high neutron pulse irradiation.
2. Neutron radiography can produce an instantaneous visual representation of the state of the flow. By using the high speed radiographic techniques, complex flow fields can be studied.
3. Neutron radiography can be used in the testing of flow and rod bundles in opaque flow channels. Because (thermal) neutrons are radiolucent to most of the channel elements.

Preliminary investigations have been made involving two component, two-phase flow system of air and water. If good results were obtained, this technique could be expanded to study bulk and subcooled boiling in rod bundles leading to

the departure from nucleate boiling. In a further application, the possibility of characterizing the quenching of a hot rod bundle by coolant can be seen.

#### 1.4 Scope of the Radiography of Two-Phase Flow

The scope of this study covers

1. The application of the OSU TRIGA reactor to neutron radiography. This includes the OSTR descriptions, beam port #3 facility, absolute flux measurement and neutron pulse operation.
2. System design of radiography which can be used to radiograph two-phase flow. Water with bubble produced by an air pump and water boiling in a steel box have been radiographed to the two-phase flow. Two different methods have been developed to radiograph these events. These use the integrated neutron flux directly exposing X-ray film in an aluminium cassette with a gadolinium foil. The other uses a scintillator to "convert" neutron into light which is then enhanced by an optical intensifier and eventually "photographed" by a high speed camera.
3. Computer codes modeling of the system have been written. The behaviors of neutrons after scattered in water with a bubble can be well-predicted by Monte-Carlo method and  $S_N$  approximation from where

predictions of the contrast between water and bubble on the film can be made. The applicability of an anti-scatter grid is also examined. The numerical predictions are also compared to the experimental results and can be useful for future study.

## II. REACTOR FACILITIES

### 2.1 Descriptions of OSTR

The TRIGA 1 MW reactor at OSU is a light water-cooled and reflected reactor using advanced TRIGA U-ZrH-moderator elements developed by Gulf General Atomic (7). This reactor is designed for continuous steady-state operation at 1 MW and may also be pulsed repetitively to yield a burst having a peak power of about 3,100 MW.

The safety of the TRIGA reactor lies in the large prompt negative temperature coefficient that is an inherent characteristic of the U-ZrH-moderator material. Thus, even when large sudden reactivity inserations are made and the reactor power rises in a short period, the excess reactivity is compensated automatically because the fuel temperature rises simultaneously so that the system returns quickly to the normal power level before any heat is transferred to the cooling water.

The OSTR utilizes solid fuel elements in which the zirconium hydride moderator is homogeneously combined with 70%-enriched uranium. The reactor core consists of a lattice of cylindrical stainless steel-clad  $\text{U-ZrH}_{1.7}$  fuel moderator elements and aluminium-clad graphite. The fuel-moderator elements have 3.5 inch long graphite end sections that form the top and bottom reflector. Water occupies about one-third of the core volume. The reactor core and core

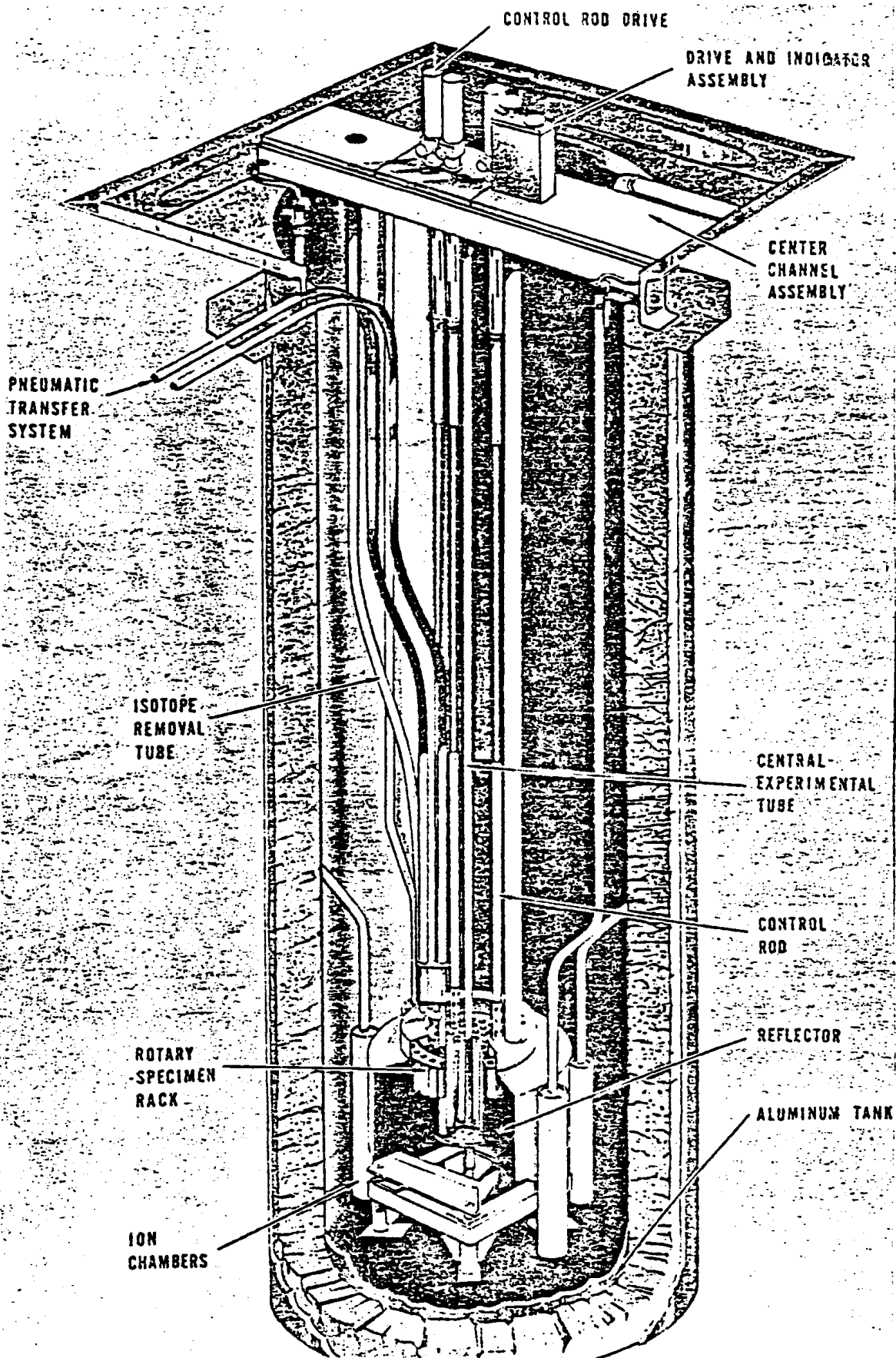


Figure 2.1 Cutaway View of TRIGA Reactor

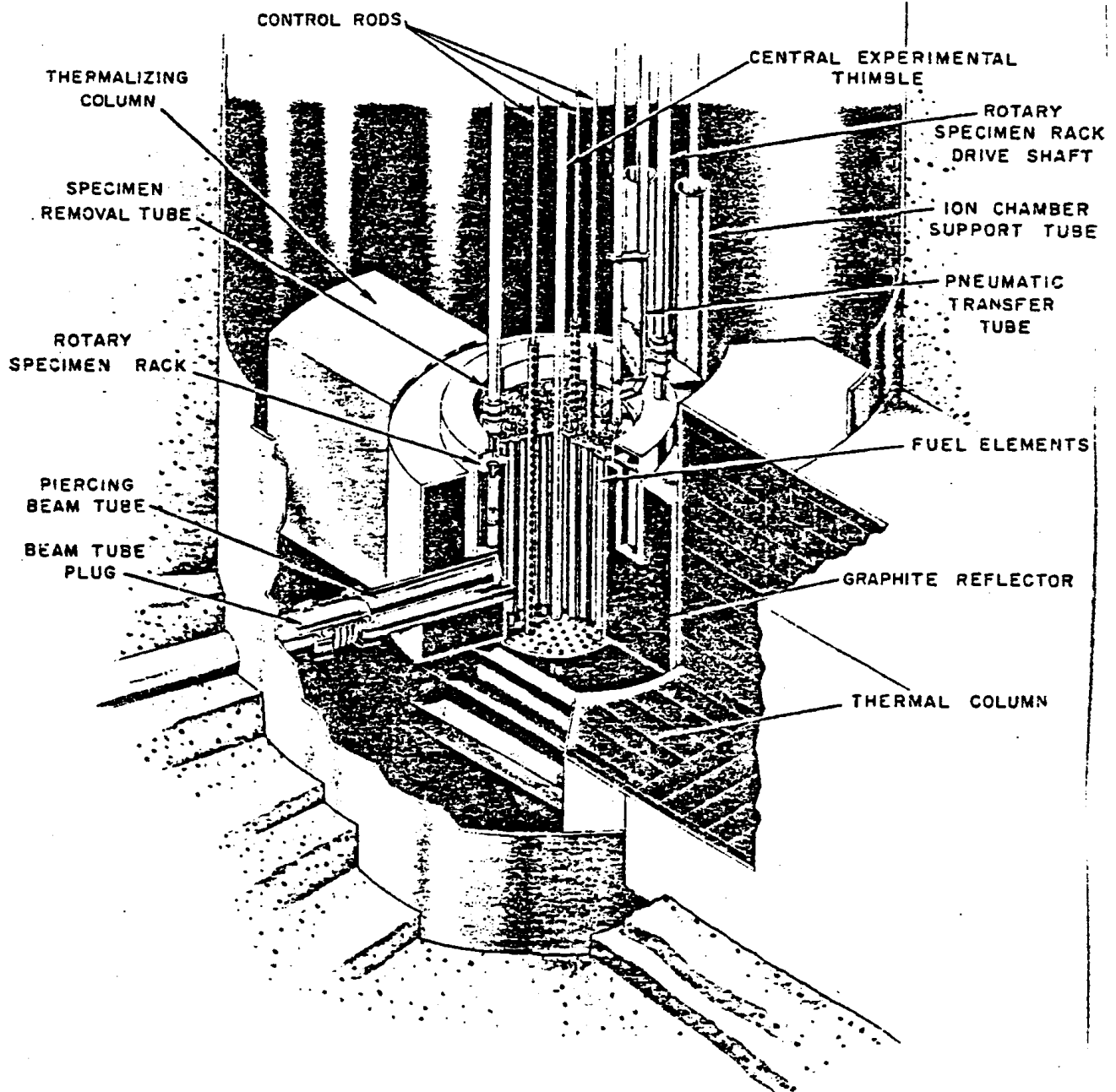


Figure 2.2 Cutaway View of TRIGA  
Reactor Core Arrangement

arrangement are shown in Figure 2.1 and Figure 2.2.

## 2.2 Beam Port #3 Facility

There are four beam ports in the OSTR. The four beam ports penetrate the concrete shield and the aluminium tank and pass through the reactor tank water to the reflector as shown in Figure 2.3. These ports provide beams of neutron and gamma radiation for various experiments. Three of these beam ports are oriented radially with respect to the center of the core, and the other port (beam port #3) is tangential to the outer edge of the core and this port is the one used in neutron radiography. Beam port #3 terminates at the outer surface of the reflector, but is also aligned with a cylindrical void which intersects the beam port #4 in the reflector graphite. The graphite voids allow the maximum radiation streaming down the port. The main reason for using beam port #3 is that this tangential port provides a radiation source giving a minimum amount of core gamma radiation which will result in the fogging of the film, because most elements, except hydrogen and very heavy elements have approximately the same mass attenuation coefficient to gamma (9).

The neutron beam path and beam port #3 are shown in Figure 2.4. The neutrons, reflected by the graphite block, go through a tank. Shutter #1 is an aluminium tank in the 6" and 8" diameter sections of the beam tube. The tank

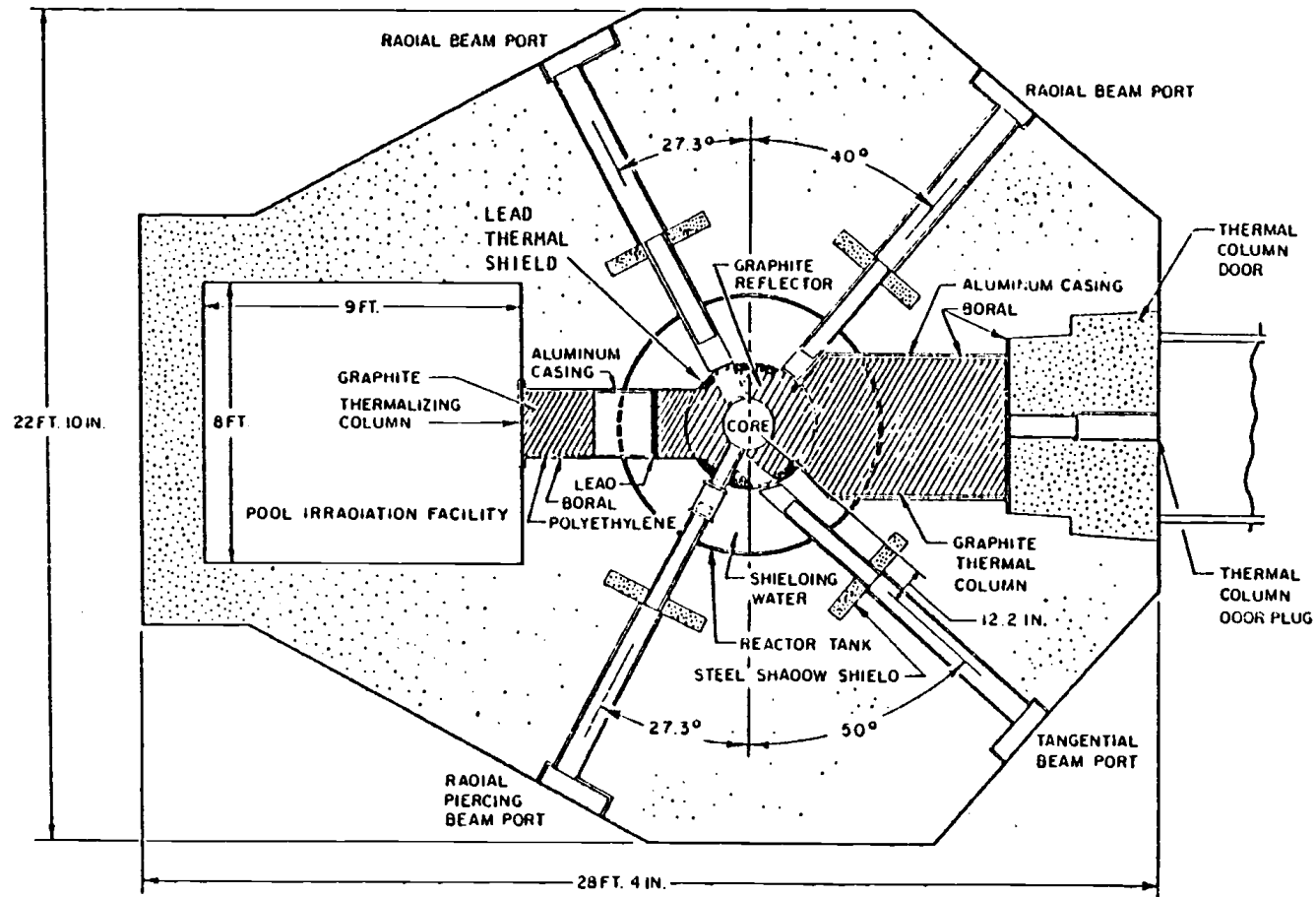


Figure 2.3 Horizontal Section of TRIGA Reactor

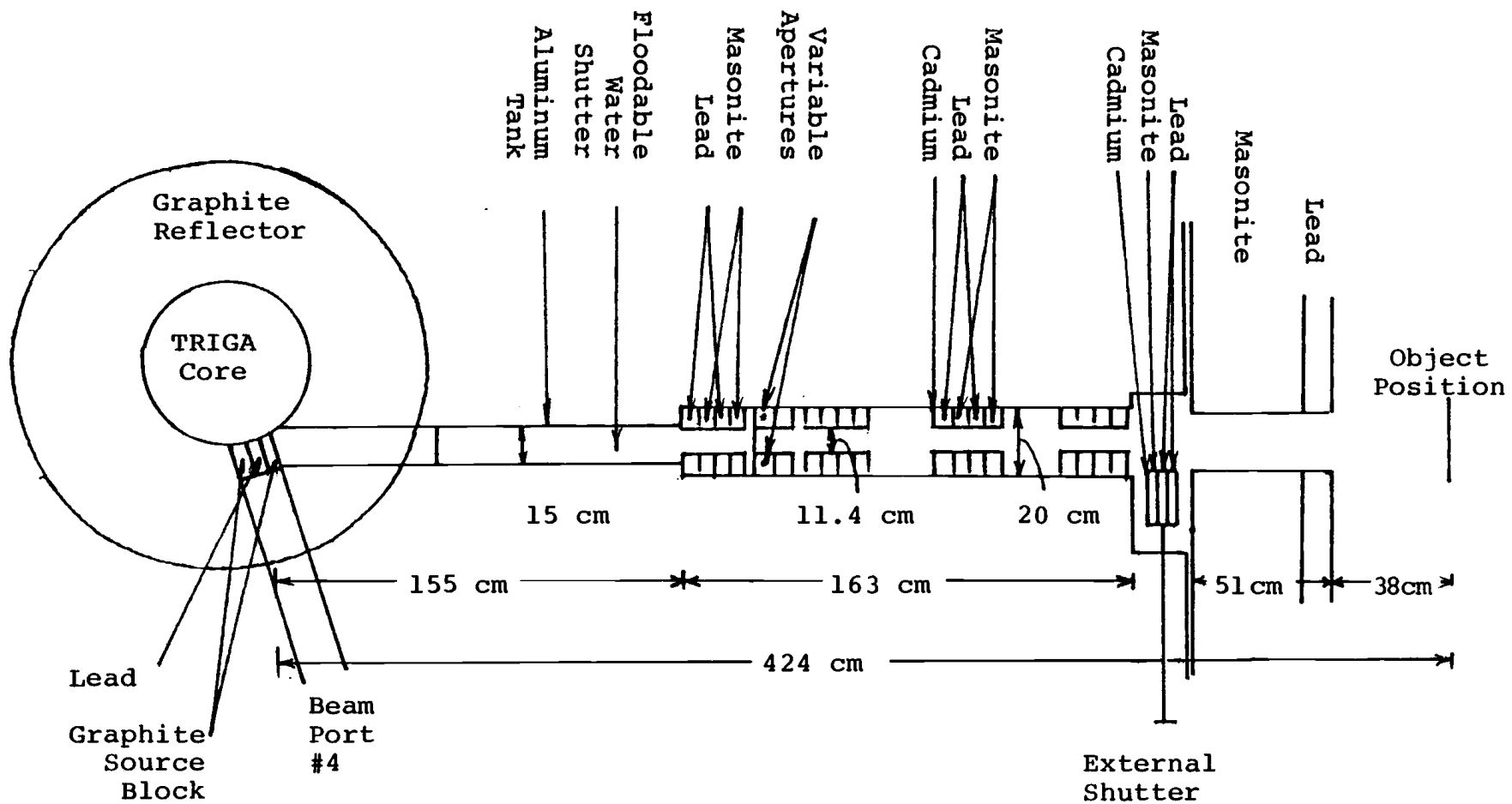


Figure 2.4 Beam Port #3 Facility

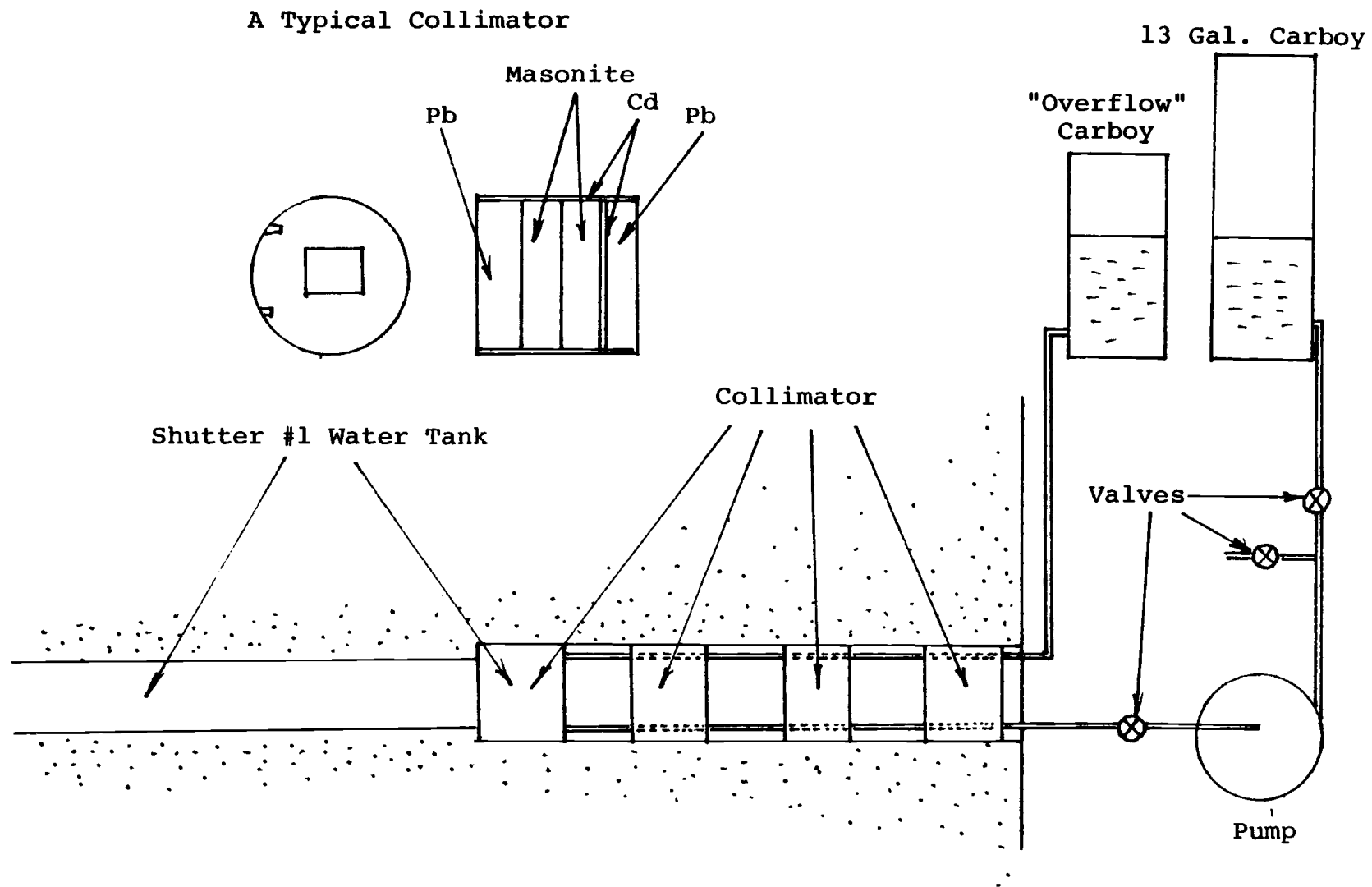


Figure 2.5 Shutter #1 and Collimators

can be filled with water, which is the "shutter closed" position and serves as the first protection for the personnel in the beam port. Figure 2.5 shows the dimension of the tank and its position in the beam tube. Before taking radiography, the shutter is emptied by a pump, which can be switched on only from the reactor control room, to a 13 gallon polyethylene carboy located on top of the external shield around the beam port. When the water shutter is open, a "BP #3 Liquid Shutter Open" annunciator is provided in the control room and a red light (indicating an open liquid shutter) is activated directly adjacent to the entrance to the BP #3 blockhouse in the operating area. After the day's exposures, the shutter is closed by draining the water from the carboy. This is done by gravity.

There is another shutter (shutter #3) which can be controlled externally. Details of this shutter can also be seen in Figure 2.4. This shutter consists of two lead and masonite 2" x 4" x 8" bricks with a cadmium surface. This shutter is manually operated by a handle from outside the shield, and it may be locked to prevent operation. Shutter open indications are also given in the control room and entrance of BP #3.

The most important component of the beam tube is the collimator. The neutron beam comes from the core, after reflection by graphite block, serves as a spherical neutron source which is of no use in neutron radiography because

of its poor resolution capability. So the neutrons must be confined in such a way that they the same direction within a tolerably small beam divergence. Because neutrons are uncharged, focusing to the degree required by utilizing the magnetic moment of the neutron is not feasible. Collimation is achieved by positioning one end of the tube lined with neutron absorber at or near the maximum thermal flux in the moderator and allowing the neutrons to stream along the tube. With reactors, adequate collimation is often given by the beam hole through the concrete biological shield. For the OSTR, there are four collimators in the beam tube. The details of the construction and position of these collimators are shown in Figure 2.4 and Figure 2.5. The collimators are made of cadmium, masonite and lead, which provide a 2" x 4" neutron beam. The first collimator is inside the water shutter #1. At the exit of the water shutter there are two cadmium-faced lead bricks with apertures in there. These apertures serve to control the intensity and divergence of the beam.

An approximate estimate of the neutron flux at the end of the collimated beam tube is given by diffusion theory as

$$\phi_c = \frac{A}{4\pi L^2} \phi \approx \frac{\phi}{4\pi (L/D)^2} \quad (2-1)$$

where A is the area of the outlet opening of the tube, L is its length (taken to be in the X direction) and L/D is

a measure of the beam diverging angle at the collimator face. The diameter is the smallest opening along the entire length. The beam intensity will therefore depend on the degree of collimation.

The resolution is obtained only at the expense of loss of neutron intensity. At OSTR, the L/D ratio is about 30:1, which means the flux will be reduced by a factor about  $10^4$  at the object position. The pulse neutron flux is about  $10^{17}$  n/cm<sup>2</sup> sec, after reduced by a factor  $10^4$ , it still gives a flux high enough for the high speed motion neutron radiography.

### 2.3 Thermal Neutron Flux Measurement

The thermal neutron flux measurement is the primary work of neutron radiography. In determining the thermal flux in BP #3, the activation method was applied. This was done by using two thin gold foils irradiated bare or covered in cadmium at 35 kW reactor power for one hour, then counted with a NaI detector and a 1024 channel analyzer to select the 412 keV gamma peak of gold. The detector efficiency at 412 keV was interpolated from test run with several standard sources as indicated in Figure 2.6. The formula used to obtain the neutron flux intensity from the gold foil count rate is

$$\phi = \frac{\lambda c}{\text{EN}\sigma(1-e^{-\lambda T})(e^{-\lambda t_1}-e^{-\lambda t_2})} \quad (2-2)$$

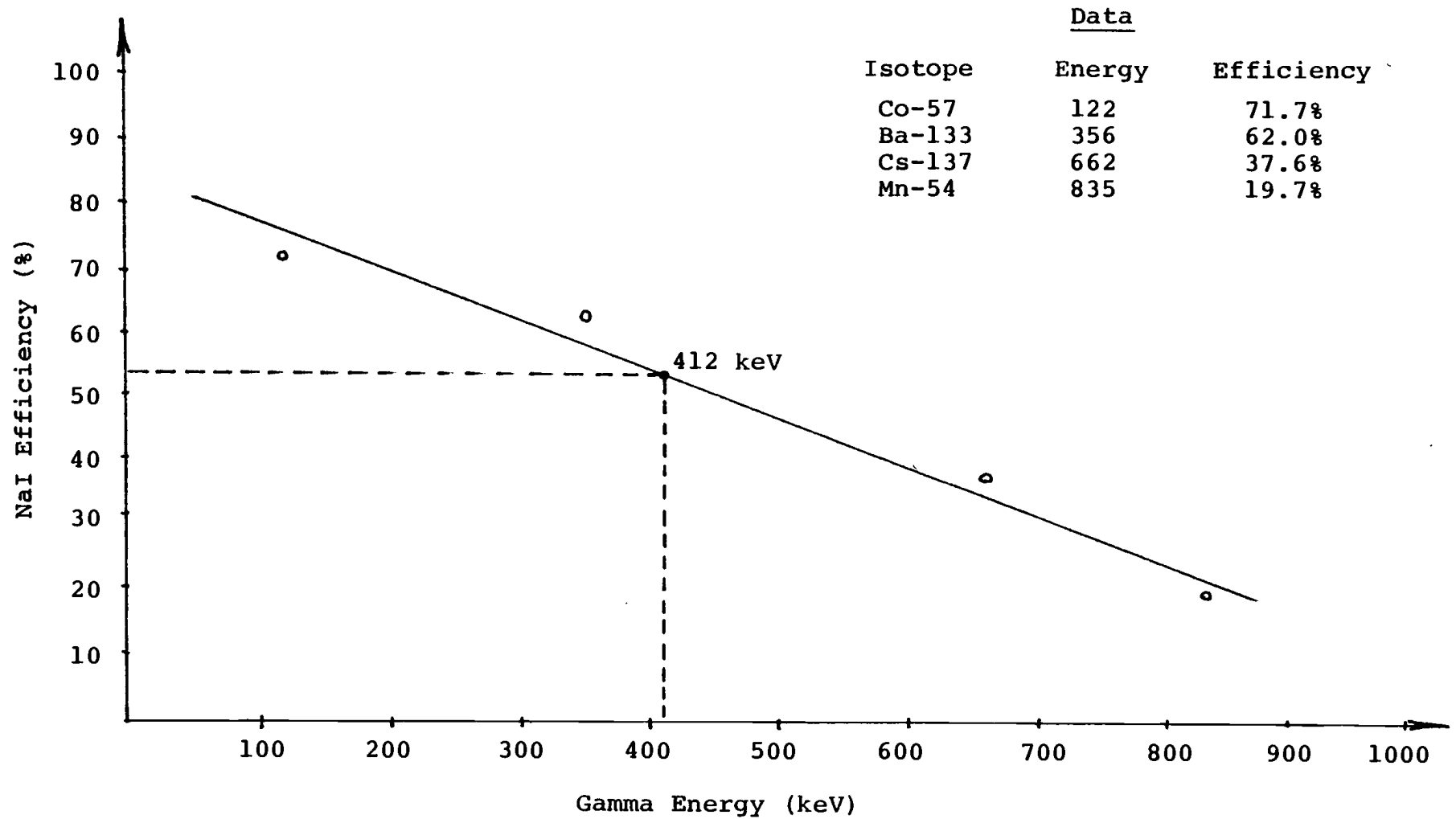


Figure 2.6 Graph of NaI Efficiency Versus Energy

where

$\lambda$  is the decay constant for gold

C is the integrated counts

E is the detector efficiency

N is the atom density of gold

$\bar{\sigma}$  is the cross-section of gold

T is the exposure time

$t_1$  is the time from EOB to start of counting

$t_2$  is the time from EOB to end of counting

The thermal neutron flux measured from this experiment was approximately  $1.12 \times 10^5$  n/cm<sup>2</sup> sec kW and cadmium ratio ( $\phi_{\text{bare}}/\phi_{\text{covered}}$ ) is 2.64.

#### 2.4 OSTR Pulse Characteristics

The main idea of using a reactor as a neutron source is its high thermal neutron beam intensity availability. Typical research reactors operate at a peak steady state flux level of  $10^{12}$  to  $10^{13}$  n/cm<sup>2</sup> sec. While this is acceptable for static radiography or very slow dynamic movement, a much higher flux is needed for very high speed movement. The OSTR provides a compact core size, a peak power level of 3,100 MW, and a peak central flux over  $10^{17}$  n/cm<sup>2</sup> sec, is very adequate for this need.

The reactor is first brought to criticality at a low power (100 w) with the transient rod in the core. The transient rod is designed to be pneumatically withdrawn

in a very short period of time. Upon rod removal, the reactor power increases to a value that produces a fuel temperature which compensates for the large excess reactivity inserted, turning the power rise around and ultimately reducing the reactor to a subcritical state. This can be done by the following operating procedures

1. Leave the transient rod disconnected from the carriage.
2. Go critical at 100 W with the other three control rods.
3. From the transient rod calibration curve, withdraw the transient rod carriage to the proper setting for the size of pulse desired.
4. Turn the range switch to 1 MW while in steady state.
5. Turn the mode selector to pulse hi ( $\geq 2.50$ ) or pulse lo ( $\leq 2.50$ ).
6. Fire the transient rod.

The time behavior of the TRIGA reactor with a large prompt negative temperature coefficient when there is a sudden insertion of a large amount of reactivity can be fairly well described by Fuchs-Nordheim model (10). This model makes two primary assumptions during the pulse

1. Delayed neutrons can be neglected.
2. All heat generated remains in the fuel. The model relates such important parameters as flux or power, reactivity, temperature change and energy released.

Let

$\phi$  = thermal flux

$\Delta k_p(t)$  = prompt reactivity change =  $\beta(\rho - 1)$

$\ell$  = prompt neutron life time

$\alpha$  = negative temperature coefficient

$T$  = temperature of the fuel

$C_p$  = specific heat per unit volume of the reactor

$E$  = total energy released per unit volume

$P(t)$  = the power as a function of time

$k_o$  = the initial step insertion of reactivity  
 $= k(0)$

$k_p(t)$  = prompt reactivity insertion  
 $= (1 - \beta)k(t)$

$\gamma$  = recoverable energy per fission

Then

$$\frac{d\phi(t)}{dt} = \frac{\Delta k_p(t)}{\ell} \phi(t) \quad (2-3)$$

$$k_p(t) = k(0)(1 - \beta)\{1 - \alpha[T(t) - T(0)]\} \quad (2-4)$$

$$P(t) = \gamma \Sigma_f \phi(t) \quad (2-5)$$

$$E(t) = \int_0^t P(t') dt' = C_p [T(t) - T(0)] \quad (2-6)$$

If  $C_p$  and  $\alpha$  are assumed to be constant, their peak power

$$P_{\max} \approx \frac{\beta^2 (\xi-1)^2 C_p}{2\alpha \ell} + P(o) \quad (2-7)$$

Temperature change

$$\Delta T(\infty) = \frac{2}{\alpha} \beta (\xi-1) \quad (2-8)$$

Total energy released

$$E(\infty) = \frac{2C_p \beta}{\alpha} (\xi-1) \quad (2-9)$$

Pulse width (full width at half maximum pulse)

$$FWHW = \frac{4\ell \cosh^{-1}(\sqrt{2})}{(\xi-1)\beta} = \frac{3.525\ell}{(\xi-1)\beta} \quad (2-10)$$

Values used for FLIP fuel in the OSTR are

$$\alpha = 13.4 \times 10^{-5} \text{ k/k } ^\circ\text{C}$$

$$\ell = 43 \text{ sec}$$

$$C_p = 720 + 1.48(T-20) \text{ Watt-sec/ } ^\circ\text{C-fuel element}$$

$$\beta = 0.007$$

The results are listed in Table 2.1.

Table 2.1 TRIGA Pulse Data

Pulse	Peak Power	FWHM
\$2.25	1,940 MW	.009 sec
\$2.00	1,300 MW	.01 sec
\$1.75	640 MW	.015 sec
\$1.50	240 MW	.025 sec

### III. HIGH SPEED MOTION NEUTRON RADIOGRAPHY

#### 3.1 System Design

The main reason for using high speed camera in neutron radiography is to freeze the image of moving object. Originally initiated by A. H. Robinson and C. R. Porter (11) this technique is called "High Speed Motion Neutron Radiography". The high speed motion system uses a broad enough neutron pulse to allow many frames to be imaged rather than a single exposure during the reactor transient.

The system diagram of high speed motion neutron radiography is shown in Figure 3.1. After the neutrons transmitted through the object, a scintillator screen and image intensifier are used and the final image record is on motion picture film. Besides the radiography of two-phase flow, the high speed motion neutron radiography is suited for radiographing the ballistic cycle of an ordnance device in which it consists of a hydrocarbon propellant inside a metal container which upon firing burns over a several millisecond period.

#### 3.2 Neutron Scintillator Screen

The scintillator screen is used to convert the spatially modulated neutrons, which are transmitted through the object, to light. The scintillator must have both a sensitive capability of forming an image with low neutron intensity and a rapid response in order that in each frame of a high

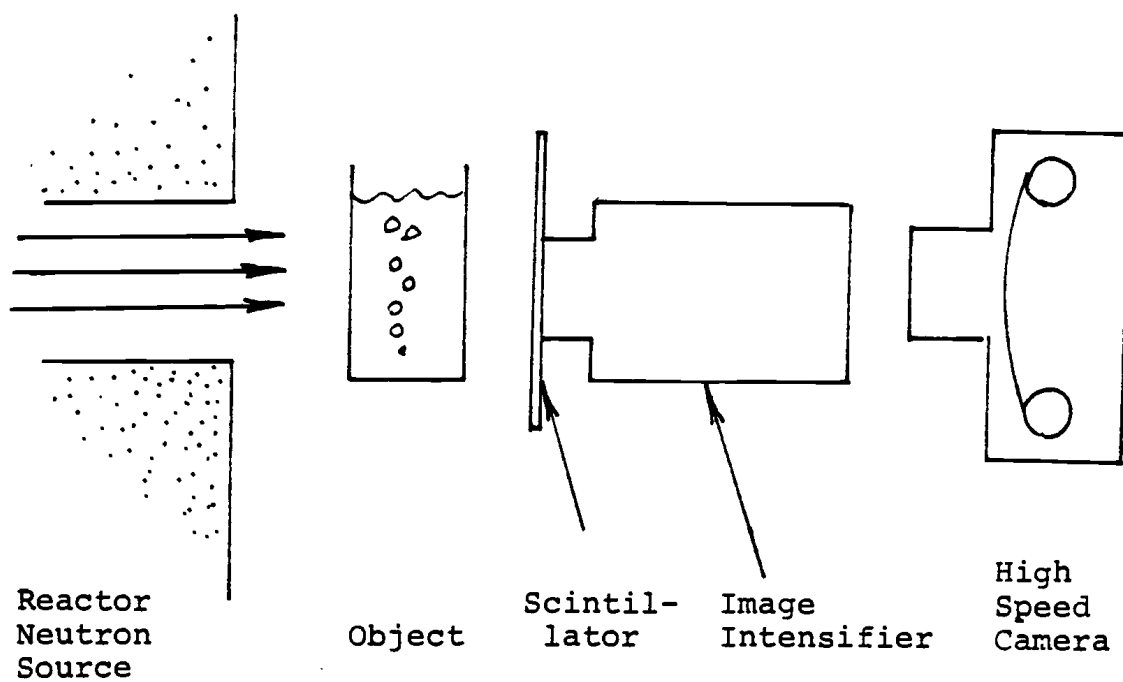


Figure 3.1 High Speed Motion Neutron  
Radiography System

speed movie be a distinct image and not a blurring of several frames together.

A variety of scintillators have been tested for use, and lithium fluoride-zinc sulphide (LiF-ZnS) scintillator have been found to be the best suited. Furthermore, a 2/1 weight ratio of ZnS to LiF in a thin layer will give the best results (12).

The lithium fluoride is enriched in its content of LiF-6, normally to 95%.

Upon the interaction with with neutron the following reaction occurs



The alpha particle and tritium nucleus will travel through the scintillator, losing their energies by excitation and ionization. These particles excite the zinc sulphide, then the light at about 450 nm wavelength will occur as the zinc sulphide crystal returns to the ground state. The construction of scintillator is described in detail in reference (5).

### 3.3 Image Intensifier

When the neutron beam passed through the scintillator screen, only 10% of the beam transmitted and it is insufficient to expose the film if the camera is focused on the scintillator screen. Therefore, an image intensifier is used to increase the light intensity. The image intensifier

is an electrooptical device which converts the incident light into electrons, accelerates the electrons across a voltage potential and scintillates the output phosphor by the highly energetic electrons. At OSU a two-stage 40 mm diameter ITT Image Intensifier is used, and the radiant power gain of this intensifier is about 300.

### 3.4 High Speed Camera and Film

A Hycam model K20S 4E rotating prism camera is used at OSU. This camera focuses on the output faceplate of the forementioned image intensifier. The camera can operate at up to 11,000 frames/sec. For radiography of two-phase flow, a frame rate of 1,000 frames/sec is used. The rotating prism system of the camera utilizes a shutter factor of 2.5 which means that at 1,000 frames/sec the exposure per frame is  $1/2.5 \times 1,000 = 0.4$  msec which is short enough to freeze the motion of bubble produced by air pump and coffee heater. The film used is Kodak RAR 2496 film; RAR 2498 can also be used.

### 3.5 Electronic Synchronization System

The electronic synchronization system is shown in Figure 3.2. For radiographing the fast moving object, the neutrons from the reactor pulse must pass through the object at the instant of the dynamic event, such as the firing of ordnance device, while the high speed camera is running at

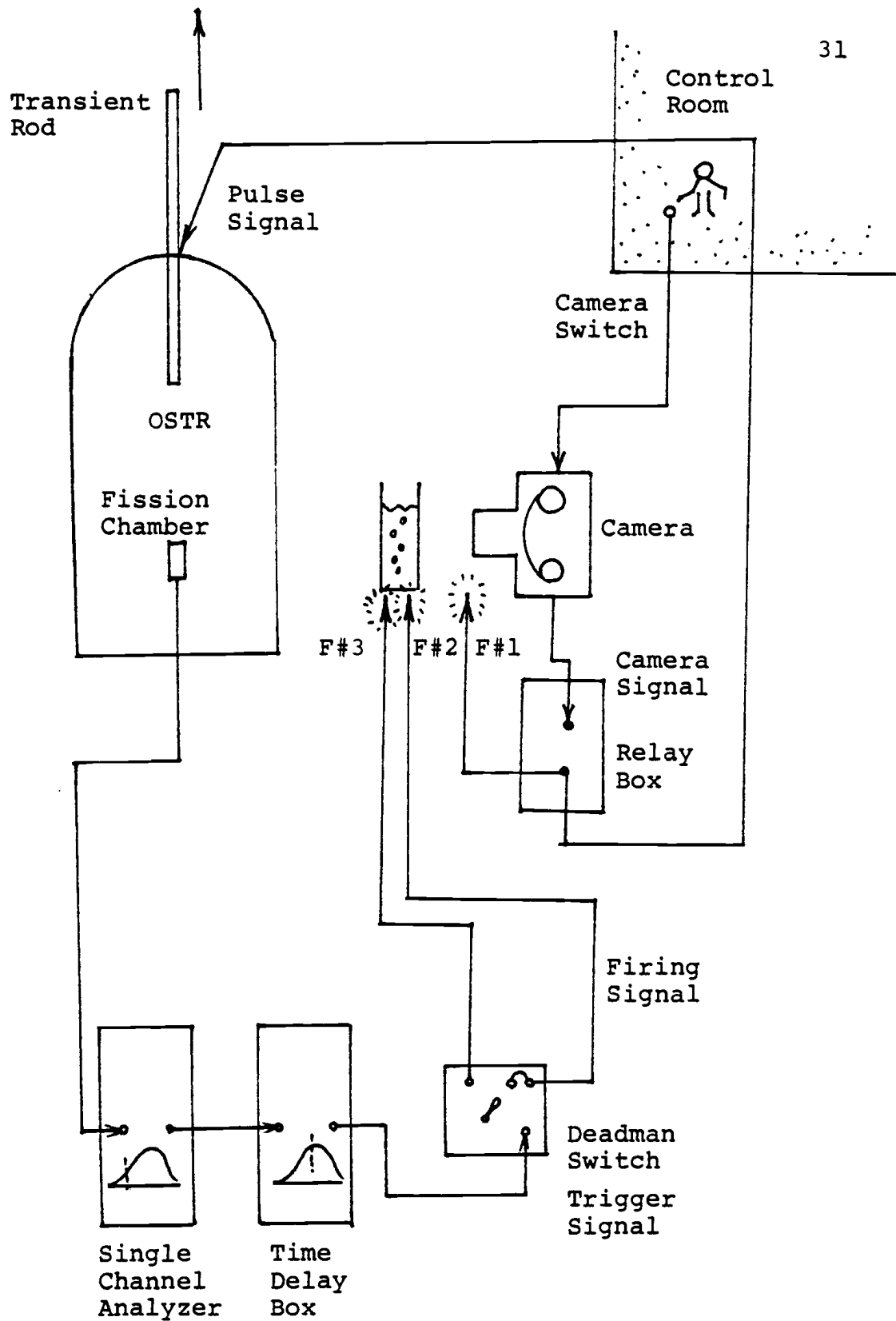


Figure 3.2 Synchronization System

the desired speed. For continuous events such as bubbles moving in the water, the reactor pulse may be signaled to occur once the high speed camera has reached the proper frame rate.

Before taking the radiographs, the reactor is taken to a low power level and prepared for the pulse initiation. The camera can only be switched on in the control room. The camera circuit is connected to a double-pole double-throw relay box which closes when the speed is reached, then sends a pulse signal to withdraw the transient rod and initiates the pulse.

If the precise measurement of the dynamic event is required, the following electronic devices are needed. First, the pulse produces an ionization voltage in the fission chamber, the voltage will exhibit a pulse shape corresponding to the neutron pulse. This voltage pulse can be chopped by the lower window in a single channel analyzer (SCA), then the time box can start the time delay from the moment that the voltage reaches the value set by the lower window of the SCA. The electronic flash guns can also be connected and triggered to indicate the actual time that the dynamic events take place.

### 3.6 Anti-Scatter Grid

The most serious problem arising in the radiography of two-phase flow is the neutron scattering in water which

then blurs the image of the bubble on the film. An anti-scatter grid is used to eliminate the scattered neutrons with angles larger than an acceptable range which depends on the  $L/D$  ratio of the grid, where  $L$  and  $D$  are the length and diameter of the grid.

The grid is usually an aluminium honeycomb plated with cadmium or indium (13). The aluminium is radiolucent to thermal neutron while cadmium and indium are the neutron opaque materials. Thus, neutrons with "incorrect" angles are absorbed. The main effect of the anti-scatter grid is to make a scatter event look like an absorption. This prevents the scattering fogging the film.

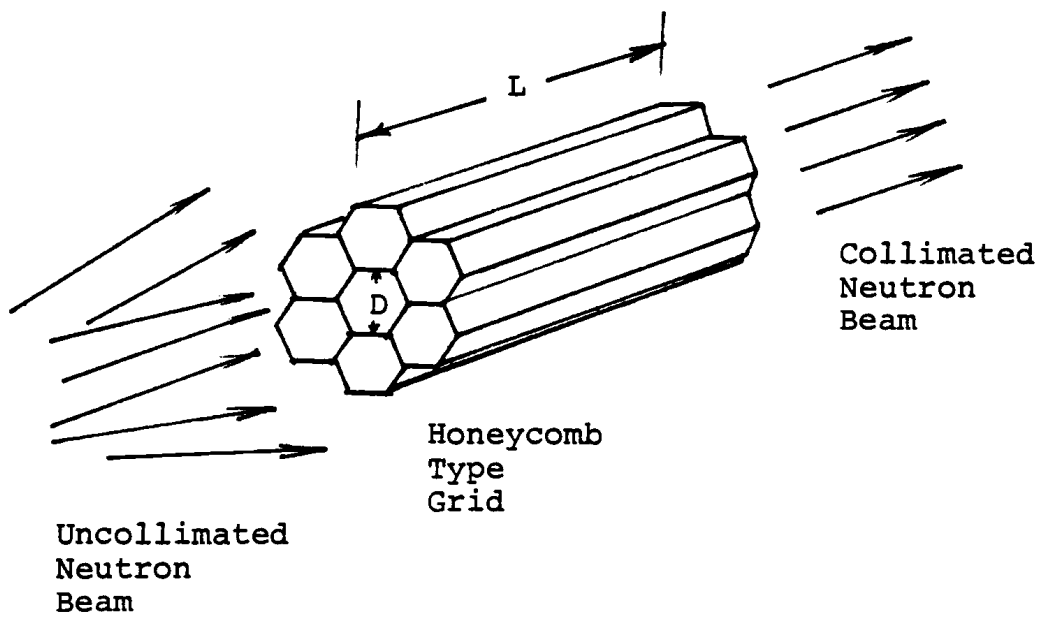


Figure 3.3 Anti-Scatter Grid

## IV. INTEGRATED FLUX PULSED RADIOGRAPHY

### 4.1 System Design

The system of the integrated flux pulsed radiography is much simpler than that of the high speed motion radiography by camera. The film is exposed in the whole pulse, and directly imaged by the ionizing radiation or light which is converted by high neutron cross-section thin foils such as gadolinium placed in a cassette. The system diagram is shown in Figure 4.1. In the integrated pulsed radiography, the motion of the object must be slow enough, so the image of the moving object will not cause much fogging on the film when the film is exposed over the time that approximately equals the FWHM of the pulse. For the OSTR, the FWHM is about 10 to 20 msec which is short enough for radiography of two-phase flow. The difference between the integrated flux pulsed radiography and the high speed motion radiography by camera is that the former is like a "snapshot" with an exposure time about 10 to 20 msec, rather than a movie. And the advantages are that the image area is much larger and an image with actual size of the object can be obtained without enlargement of the film.

### 4.2 Gadolinium Foil and X-ray Film

Gadolinium foil is the most suited material in the direct imaging technique. Gadolinium has the thermal

neutron absorption cross-section high up to 50,000 barns. Neutrons absorbed in the foil generate beta radiation (internal conversion electrons) which directly exposes the film. The foil is placed in a cassette made of aluminum. There are two kinds of films used, Kodak T-5 and DR-5. T-5 gives better sensitivity while DR-5 gives better resolution.

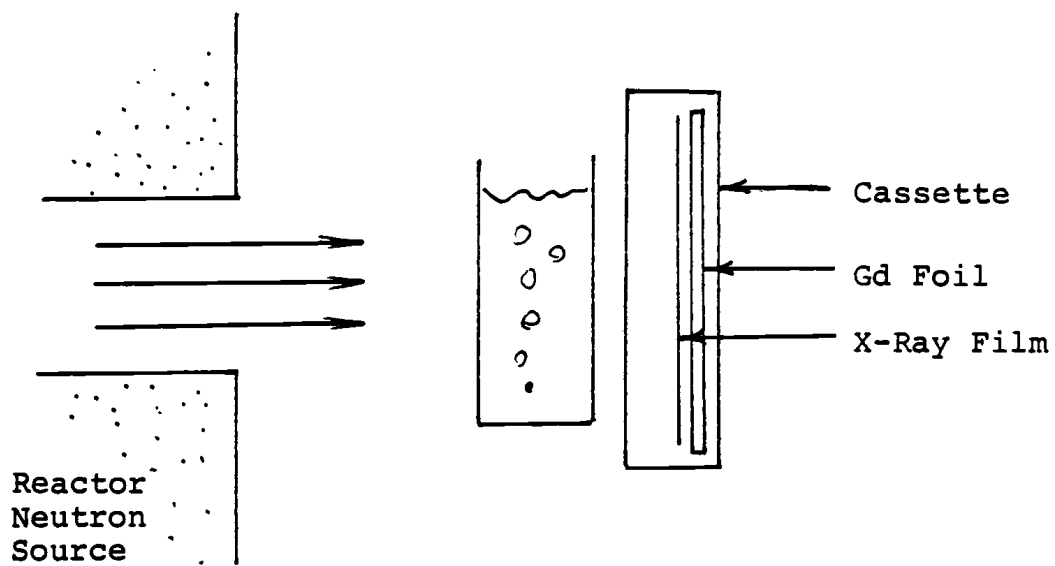


Figure 4.1 Integrated Flux Neutron Radiography System

## V. COMPUTER MODELINGS OF THE SCATTERING SYSTEM

Computer calculations have been used to calculate the intensity ratios of the image of the bubble to that of water on the film with variable thickness of water and bubble. These calculations were also performed to predict any significant improvements possible by using an anti-scatter grid.

### 5.1 S<sub>N</sub> Approximation Method

By assuming that the neutron energy does not change in scattering collisions, the neutrons scattered in water can be described by the one-speed neutron transport equation (14) as

$$\frac{1}{v} \frac{\partial \phi}{\partial t} + \hat{\Omega} \nabla \phi + \Sigma_t(r) \phi(r, \hat{\Omega}, t) = \int_{4\pi} d\hat{\Omega}' \Sigma_s(\hat{\Omega} \rightarrow \hat{\Omega}) \phi(r, \hat{\Omega}', t) + s(r, \hat{\Omega}, t) \quad (5-1)$$

Then assume both isotropic neutron sources (if any)

$$s(r, \hat{\Omega}, t) = \frac{1}{4\pi} S(r, t) \quad (5-2)$$

and isotropic scattering (in LAB system)

$$\Sigma_s(\hat{\Omega}' \rightarrow \hat{\Omega}) = \frac{1}{4\pi} \Sigma_s \quad (5-3)$$

But, although neutron scattering is usually isotropic in the CM system, it is far from isotropic in the LAB system, particularly for low mass number scatterers such as hydrogen. In the next section, the anisotropic scattering will be taken into account in Monte Carlo method.

In steady-state and planar symmetry, the one-speed neutron transport equation can be simplified to the equation

$$\mu \frac{\partial \phi}{\partial x} + \Sigma_t \phi(x, \mu) = \frac{\Sigma_s}{2} \int_{-1}^{+1} d\mu' \phi(x, \mu') + \frac{S(x)}{2} \quad (5-4)$$

where  $\mu = \cos\theta$ . This equation can be solved numerically by discretizing the ordinate (angles). Assume the flux is constant in each discretized angle  $\mu_j$ , then

$$\mu_j \frac{\partial \phi}{\partial x} \phi(x, \mu_j) + \Sigma_t \phi(x, \mu_j) \approx \frac{\Sigma_s}{2} \sum_{i=1}^N \omega_i \phi(x, \mu_i) + \frac{S(x)}{2} \quad (5-5)$$

where the Gaussian integration is used

$$\int_{-1}^{+1} \phi(x, \mu) d\mu \approx \sum_{i=1}^N \omega_i \phi(x, \mu_i) \quad (5-6)$$

and  $N$  is the order of discretization. The difference equation can be obtained by dividing the scattering region into  $K$  intervals and integrating it from  $X_k$  to  $X_{k+1}$

$$\begin{aligned}
& \mu_j [\phi(X_{k+1}, \mu_j) - \phi(X_k, \mu_j)] + \frac{\Delta X_k}{2} \Sigma_t [\phi(X_{k+1}, \mu_j) + \phi(X_k, \mu_j)] \\
&= \frac{\Sigma_s}{4} \sum_{i=1}^N \omega_i [\phi(X_{k+1}, \mu_i) + \phi(X_k, \mu_i)] \Delta X_k + \frac{\Delta X_k}{4} (\Sigma_{kH} + \Sigma_k) \\
&= Q_k \text{ (RHS)} \tag{5-7}
\end{aligned}$$

Solve for  $\phi_{k+1,j}$

$$\phi_{k+1,j} = \frac{[1 - \frac{\Sigma_t \Delta X_k}{2\mu_j}]}{[1 + \frac{\Sigma_t \Delta X_k}{2\mu_j}]} \phi_{k,j} + \frac{Q_k}{\mu_j [1 + \frac{\Sigma_t \Delta X_k}{2\mu_j}]} \tag{5-8}$$

for  $\mu_j > 0$

$$\phi_{k,j} = \frac{[1 + \frac{\Sigma_t \Delta X_k}{2\mu_j}]}{[1 - \frac{\Sigma_t \Delta X_k}{2\mu_j}]} \phi_{k+1,j} - \frac{Q_k}{\mu_j [1 - \frac{\Sigma_t \Delta X_k}{2\mu_j}]} \tag{5-9}$$

for  $\mu_j < 0$

The solution is obtained by starting with known values of the flux at  $X = 0$  and calculating the flux for every discrete angle and space point throughout the entire region, then calculating a new source ( $Q$ ) and solving for the new fluxes. This iteration on  $Q$  continues until  $Q$  is converged at all space points.

To simplify the problem the calculations were performed for an infinite slab geometry. The geometry for the calculation is shown in Figure 5.1.

The calculations of the incident neutron intensity have been selected for the  $S_{10}$  case (i.e., 10 angles). With the assumption that  $N = 10$  is the angle of the incident beam ( $\theta \sim 0$ ), the boundary condition is

$$\phi(0,10) = 1.0 \quad . \quad (5-10)$$

Also angles 1 to 5 which cover the left half solid angle are negatively directed angles and angle 6 to 10 which cover the right half solid angle are positively directed angles relative to any position in the object. The predicted flux on the right faceplate, which exposes the film, can be represented by integrating the differential fluxes at  $x = W$  over angle  $\mu_j$ . If an anti-scatter grid is used, only the flux with small diverging angle ( $\theta \sim 0$ ) can pass through the grid without being absorbed by the grid, and eventually be detected and exposes the film. This flux is  $(W, 10)$ , where  $W$  is the thickness of the water. For the case that there is a bubble with "thickness"  $D$  in the water, the calculations are still the same except the cross-section of the water is changed to 0 in the bubble region. The computer code is listed in Appendix I.

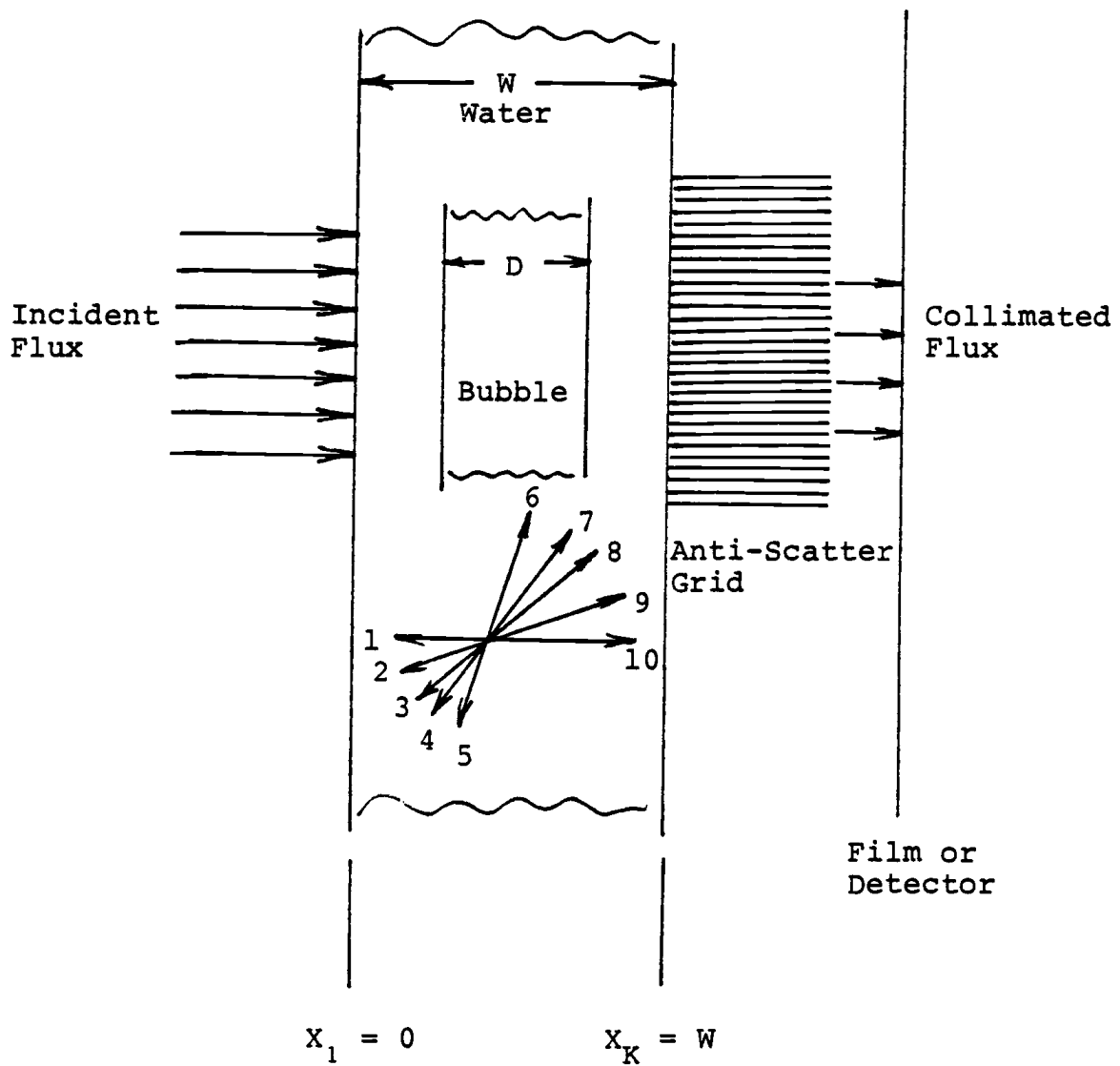


Figure 5.1 Geometry of  $S_N$  Approximation

## 5.2 Monte Carlo Method

The Monte Carlo method, which has proved to be useful in some areas of reactor physics, is a numerical procedure based on statistical (or probability) theory. In neutron transport calculations, the applicability of the Monte Carlo technique arises from the fact that the macroscopic cross-section may be interpreted as a probability of interaction per unit distance traveled by a neutron. Thus, in the Monte Carlo method, a set of neutron histories is generated by following individual neutrons through successive collisions. The locations of actual collisions and the results of such collision, e.g., direction and energy of the emerging neutrons, are determined from the range of possibilities by sets of random numbers. For example, an azimuthal angle can be chosen as  $\theta = 2\pi \cdot \text{RN}$  and the cosine of a polar<sup>\*</sup> angle as  $\mu = 2 \cdot \text{RN} - 1$ ; the reason is that the source is isotropic and all values of  $\theta$  and  $\mu$  are equally probable in the intervals  $0 \leq \theta \leq 2\pi$  and  $-1 \leq \mu \leq 1$ , respectively.

The geometry of Monte Carlo method which simulates the scattering of neutron in water with a bubble located in the center is shown in Figure 5.2. In this model, the following assumptions were made

1. Batches of incident neutrons are localized in K intervals along the Y-direction on the left face-plate of the water.

\* In this coordinate system, the polar angle  $\theta$  is measured from the incoming neutron direction. Then,  $\mu = \cos \theta$ .

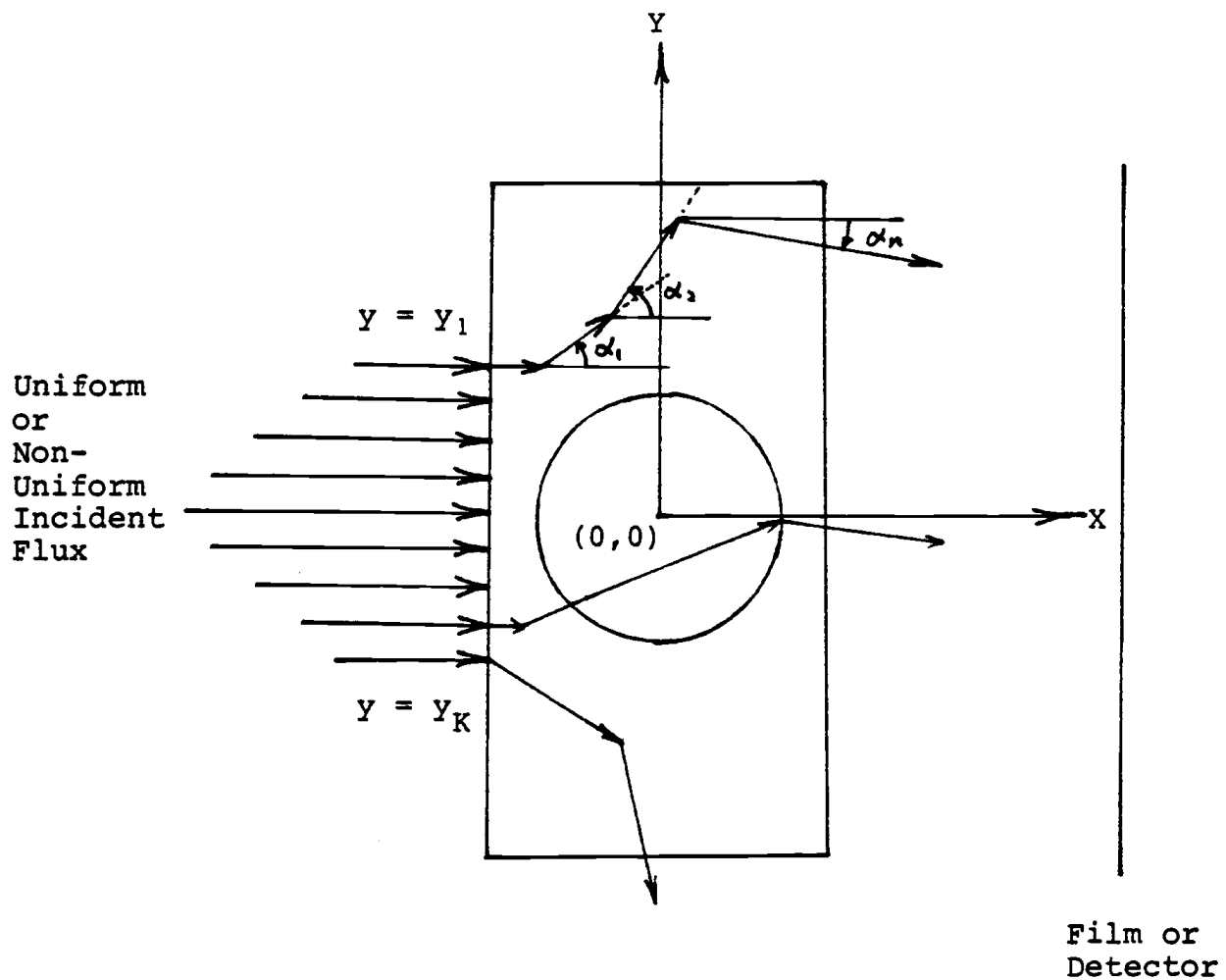


Figure 5.2 Geometry of Monte Carlo Method

2. The scattering angle of each collision is assumed to be a constant and equals  $\cos^{-1}(\bar{\mu})$ , where  $\bar{\mu} = 0.324$ .

To start the calculation, the incident neutron flux distribution must be determined, because it directly affects the image of the bubble, and in fact, the beam is not very uniform as shown by the radiographic density contours in Figure 5.3 (15). In each batch, the neutron histories are chosen to be 500 to 1,000 or higher.

Because the scattering of neutron in water is not isotropic, i.e.,  $\bar{\mu} = 0.324$ , therefore the equation  $\mu = 2*RN-1$  can not be used. Assume a neutron moves the distance  $P_0$  with a scattering angle equal to zero before having its first collision. As a result of this collision, the neutron is scattered through the angle  $\theta_1$ , as shown in Figure 5.4, and then travels another distance  $P$  in this direction before it has a second collision. As indicated in the figure, this is equivalent to moving the distance  $P_1 \cos \theta_1$  in the original direction. At the second collision the situation is more complicated. The angle of scattering,  $\theta_2$ , is measured from the direction of the second travel path, and the distance which the neutron travels in its original direction before a third encounter is now  $P_2 \cos \alpha$ , where  $\alpha$  is the angle between the direction of motion after the second collision and the original direction. It can be shown that

$$\cos \alpha = \cos \theta_1 * \cos \theta_2 + \sin \theta_1 * \sin \theta_2 * \cos \phi_2 \quad (5-10)$$

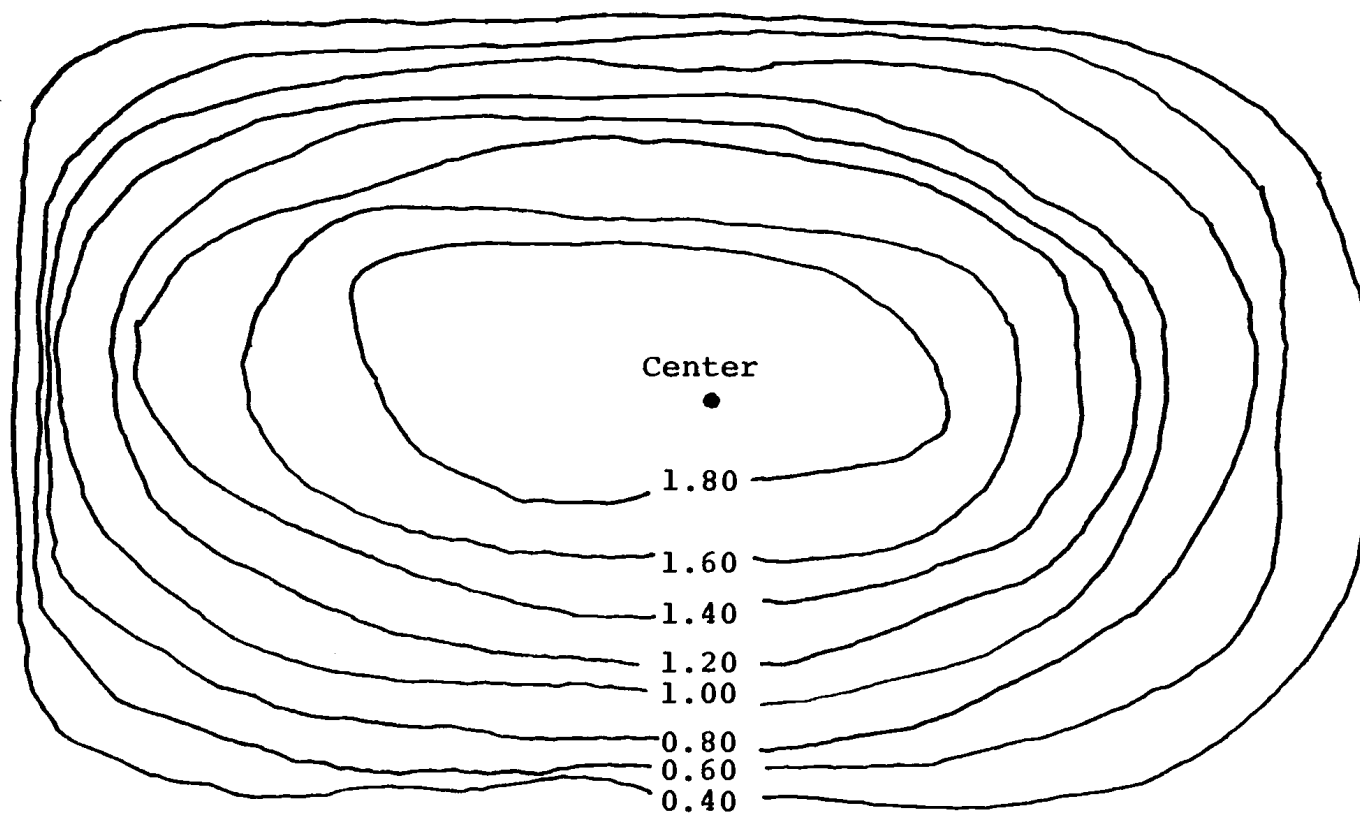


Figure 5.3 Flux Density Contours for BP #3  
at Object Position (actual size)

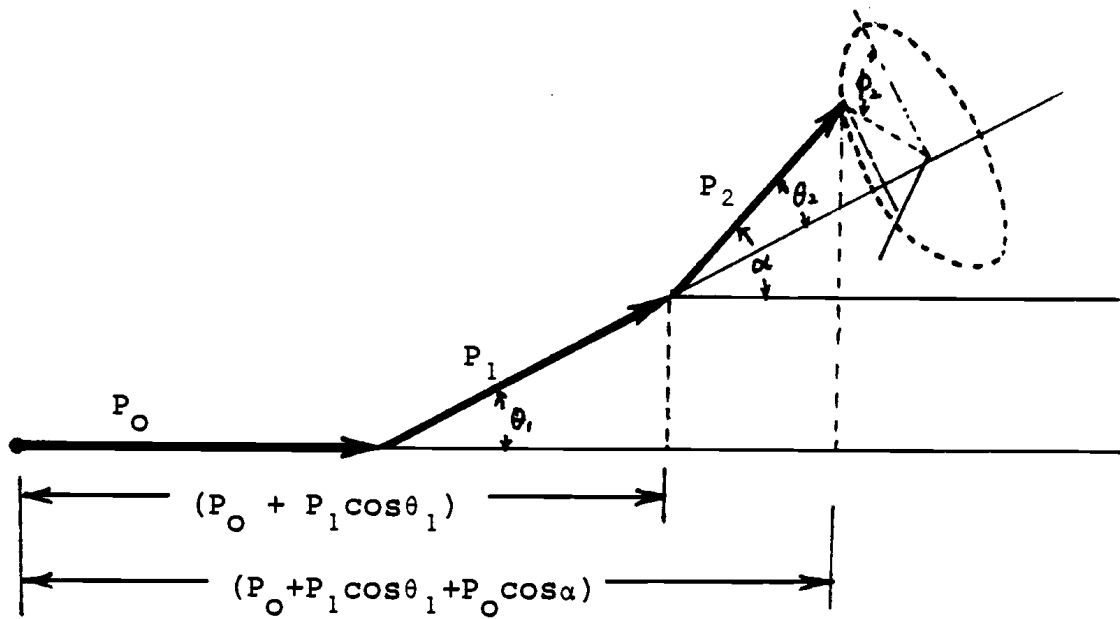


Figure 5.4 Diagram of Anisotropic Scattering

where  $\phi_2$  is the angle of rotation of  $P_2$  with respect to the plane of the first two paths. With the assumption that the scattering angle of each collision yields  $\theta = \cos^{-1}(\bar{\mu})$ , this problem can be simplified to a great extent.

The neutron path length is calculated by

$$P = (-1./\Sigma_t) * \log(RN) \quad (5-11)$$

The angle of rotation is calculated by

$$\phi = 2\pi * RN \quad (5-12)$$

and the new position of the neutron after each collision can be determined by

$$X_{\text{new}} = X_{\text{old}} + P * \cos\alpha \quad (5-13)$$

$$Y_{\text{new}} = Y_{\text{old}} + P * \sin\alpha \quad (5-14)$$

The difference between bubble and water is the cross-section. When a neutron is scattered into the bubble, the incident angle will be preserved and the neutron goes in a straight way without scattering until it hits the other side of the bubble and starts another scattering in the water. Due to the different scattering mechanism, the contrast of the images between bubble and water can be shown on film. To count the neutrons that expose the film on the right face-plate of the water, the traveling path of each neutron must be traced. If the neutron leaks out in a place other than

the film, another neutron history is begun. The neutrons counted are also localized in K intervals on the right faceplate of the water depending on the position they come out. The exposure of the film will obviously depend on the transmitted and localized neutron intensities. In this program, an anti-scatter grid can also be simulated. If D/L is the ratio of the diameter to the length of the grid, then only the outgoing neutrons with spatial angle  $\text{SIN}^{-1}(D/L)$  can pass through the grid, the others will be absorbed in the grid. This is simulated in the code by only counting those neutrons emerging from the right faceplate with angles less than a specified value. Using this code, the improvement in image contrast between the bubble and the water with anti-scatter grid has been calculated. These results are compared to measured values in the next chapter. The Monte Carlo code is listed in Appendix II.

## VI. RESULTS AND CONCLUSIONS

### 6.1 Results

The system of high speed motion neutron radiography at OSU has demonstrated the feasibility of radiographing two-phase flow. In radiographing two-phase flow, several different combinations have been arranged according to container, type of two-phase condition, liquid and radiographic method. Figure 6.1 shows the two steel boxes used as containers. The dimensions of these boxes are  $5/4" \times 4" \times 5"$  and  $5/16" \times 4" \times 5"$  and the thickness of steel is  $1/8"$ . The reason for using steel is that most coolant channels are made of steel alloys and steel is radiolucent to a neutron beam. Figure 6.2 shows two devices, an air pump and a heating element, which produced the two different kinds of two-phase flow under study: bulk water with air bubbles; and boiling of water. The heating element, which simulates the fuel rod in a reactor, has a thermal output (linear rating) of approximately 0.6 kW/ft, which is about 10 to 20 times smaller than that of a real fuel rod. The speed of bubbles is about 10 to 20 cm/sec for the air pump and about 20 to 50 cm/sec for the heating element. The images of the bubbles were frozen using the high speed movie radiography camera while some blurring occurred in the integrated flux pulsed (flash) radiography. In addition to the light water, heavy water ( $D_2O$ ) was also used for radiography. Since the macroscopic cross-section of heavy water ( $\Sigma_s = 0.449 \text{ cm}^{-1}$ ) is much smaller than that of water ( $\Sigma_s = 3.45 \text{ cm}^{-1}$ ), the visibility of the image, which is obscured by the great number of neutrons scattered at large angles,

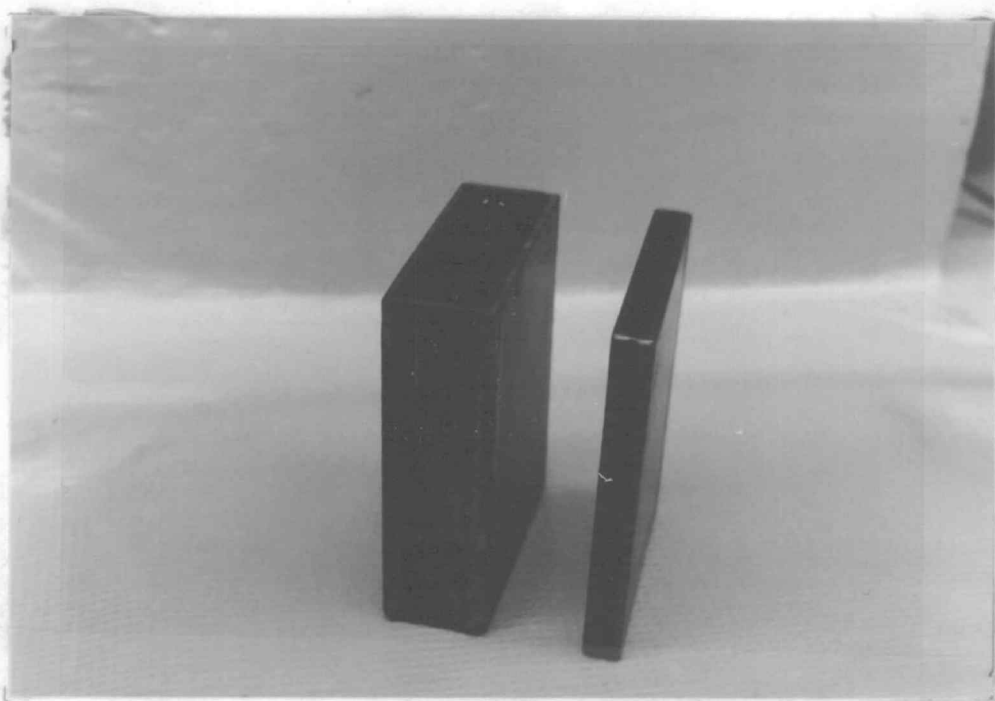


Figure 6.1    Steel Boxes  
Thick Box:  $5/4'' \times 4'' \times 5''$   
Thin Box:  $5/16'' \times 4'' \times 5''$



Figure 6.2    Air Bubble Pump and Heating Element

was greatly improved by using heavy water.

The integrated flux pulsed radiographs of two kinds of flow (water with air bubbles and boiling) of water and heavy water in  $5/4$ "- and  $5/16$ "-thick boxes are shown in figures 6.3 through 6.13. Figure 6.3 is the air pumped into water in the thick box with a  $5/2$ " X 2" cadmium window. Figure 6.4 is the boiling water in the thick box. Neither of these two figures can show the bubbles clearly in the thick box due to the large amount of scattering of neutrons. Only the bubbles on the surface can be seen in figure 6.3. A small bubble on the heating loop can be seen in figure 6.4. Figure 6.5 through figure 6.7 show the air pumped into water in the thin box. The visibility of the bubbles has been improved significantly by reducing the thickness of water and hence the scattering of the neutrons. In figure 6.6 and figure 6.7, a 1" X  $1/2$ " cadmium window is used, which confines the radiographed area. Two thin cadmium wires are glued in the window in order to indicate the orientation of the neutron beam. All the pictures are taken in the direction that the object will "be seen" by the neutron beam. In figure 6.7, there is a 2" gap between the box and the film. This allows neutrons with large scattering angles to miss the imaging film. This gap functionally serves as an anti-scatter grid. Compared with figure 6.6 and figure 6.7, it can be seen that the contrast between bubbles and water in figure 6.7 is significantly enhanced, but at the expense of losing the image sharpness due to the longer distance between the object and the film. Figure 6.8 and figure 6.9 show the boiling water in the thin box. In figure 6.8, some small bubbles are on the loop

showing beginning of boiling. This boiling is the nucleate boiling region. Figure 6.9 shows the fully developed boiling of water. Part of the heating element in figure 6.9 is in the film boiling region. While attempting to get this radiograph of film boiling, one of the heating elements burned out, as would be expected in such situations. Figure 6.10 and figure 6.11 show the heavy water with bubbles and boiling in thick box, a situation that was not visible when radiographing the light water. The same flow (air in water and boiling) are shown in figures 6.12 and 6.13 using heavy water in the thin box. In figure 6.13, the materials in the heating element and the electric wire are also shown.

The motion neutron radiography movies of two-phase flow of light water in the thin box are shown in figure 6.14 through figure 6.19. Figure 6.14 shows the water with air bubbles taken with a camera frame rate of 5000 frames/sec and pulse peak power of 3080 MW. Figure 6.15 shows the boiling of water with a camera frame rate of 2000 frames/sec and pulse peak power of 3100 MW. Figure 6.16 shows the boiling of water with a camera frame rate of 1000 frames/sec and pulse peak power of 3140 MW. Figure 6.17 shows the boiling of water with a camera frame rate of 500 frames/sec and pulse peak power of 3120 MW. In figures 6.18 and 6.19, pulse peak powers are decreased down to 187 MW and 116 MW and camera frame rates are slowed down to 250 and 125 frames/sec respectively. The rising of the bubbles can be seen in figure 6.14. The boiling of water can be seen in figures 6.17 and 6.16 but the intensifier quenched due to the strong light input. In figure 6.18 and figure 6.19, the exposure

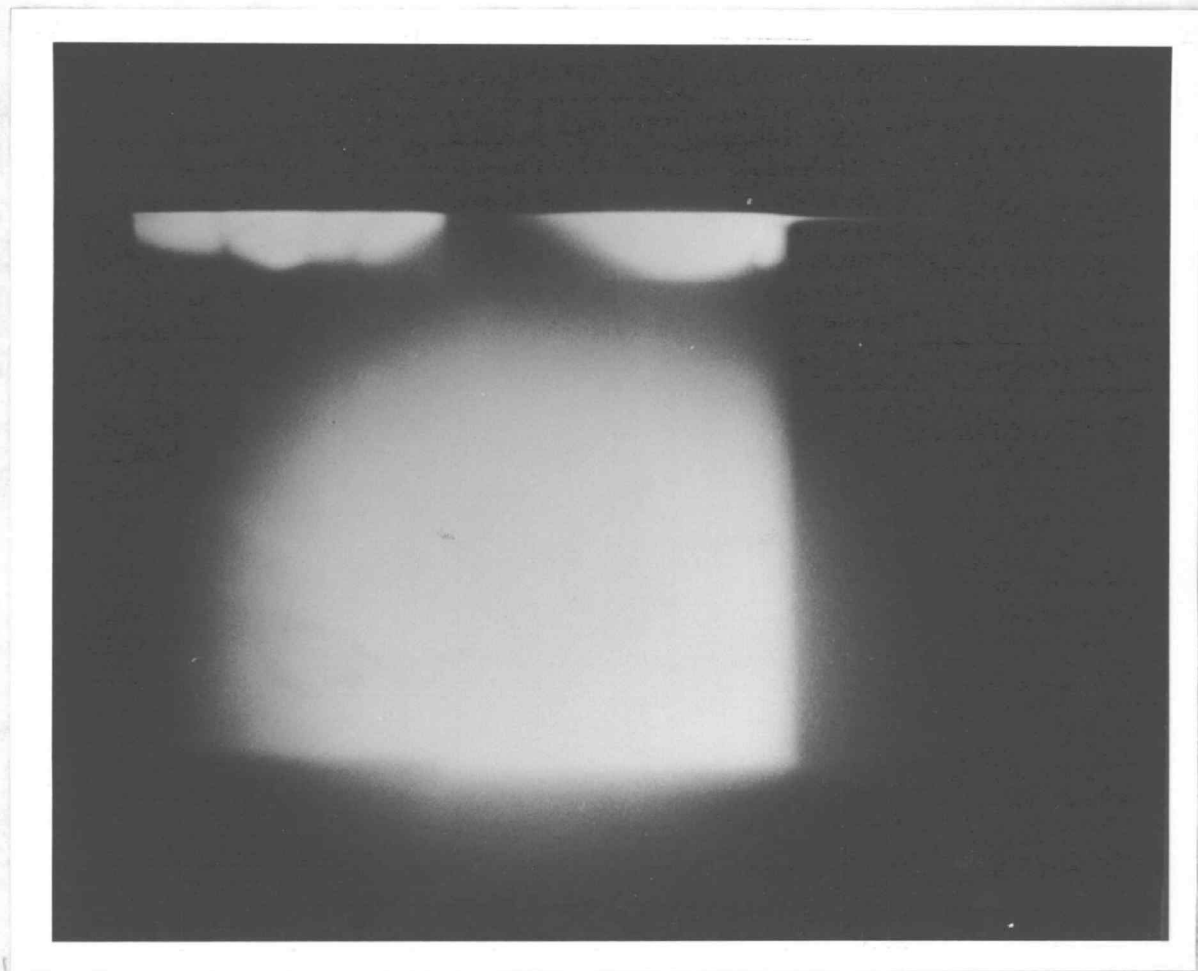


Figure 6.3 Integrated Flux Pulsed Radiography  
H<sub>2</sub>O with Air Bubbles in Thick Box  
Peak Power: 1,540 MW

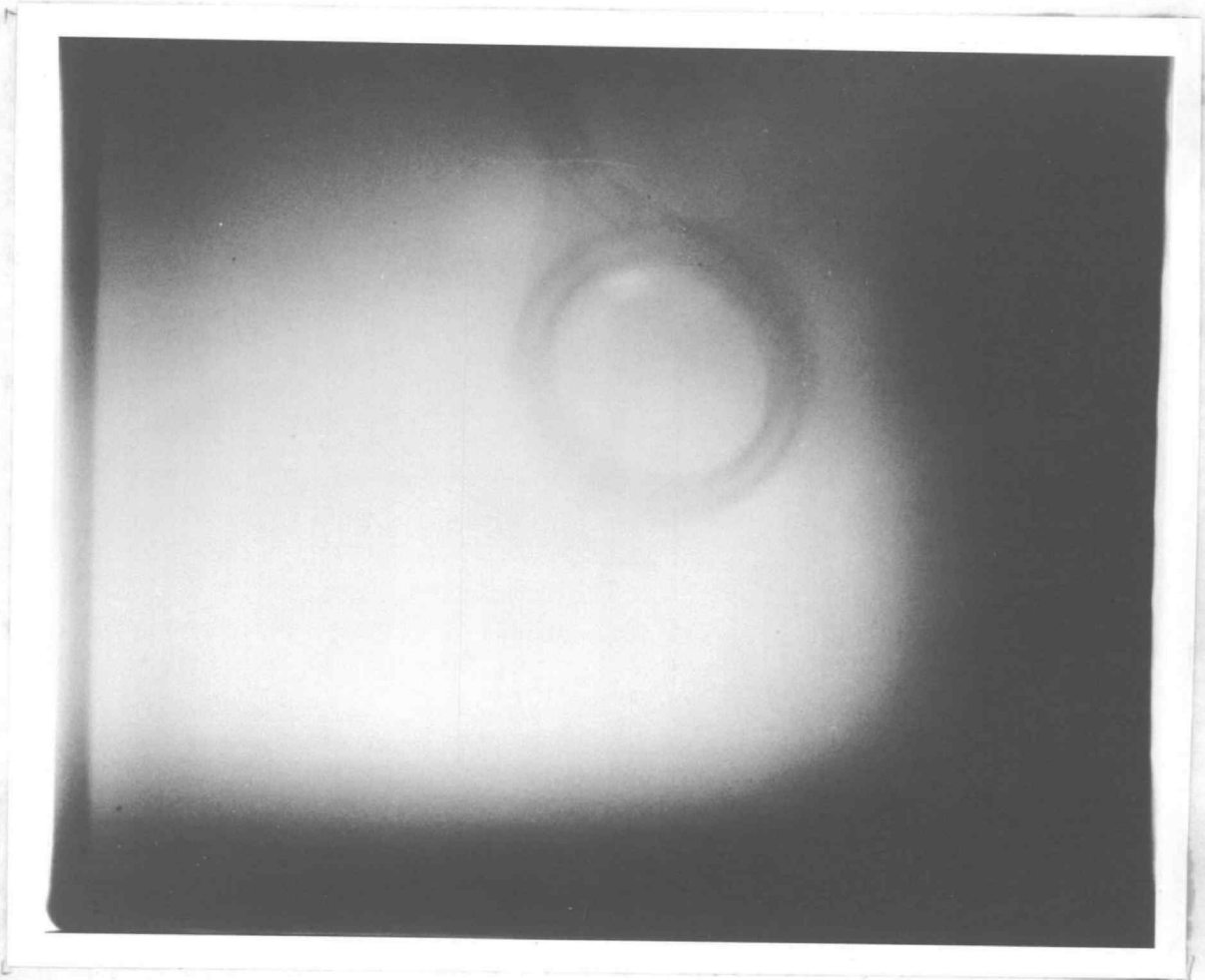


Figure 6.4 Integrated Flux Pulsed Radiography  
H<sub>2</sub>O Boiling in Thick Box  
Peak Power: 3,100 MW

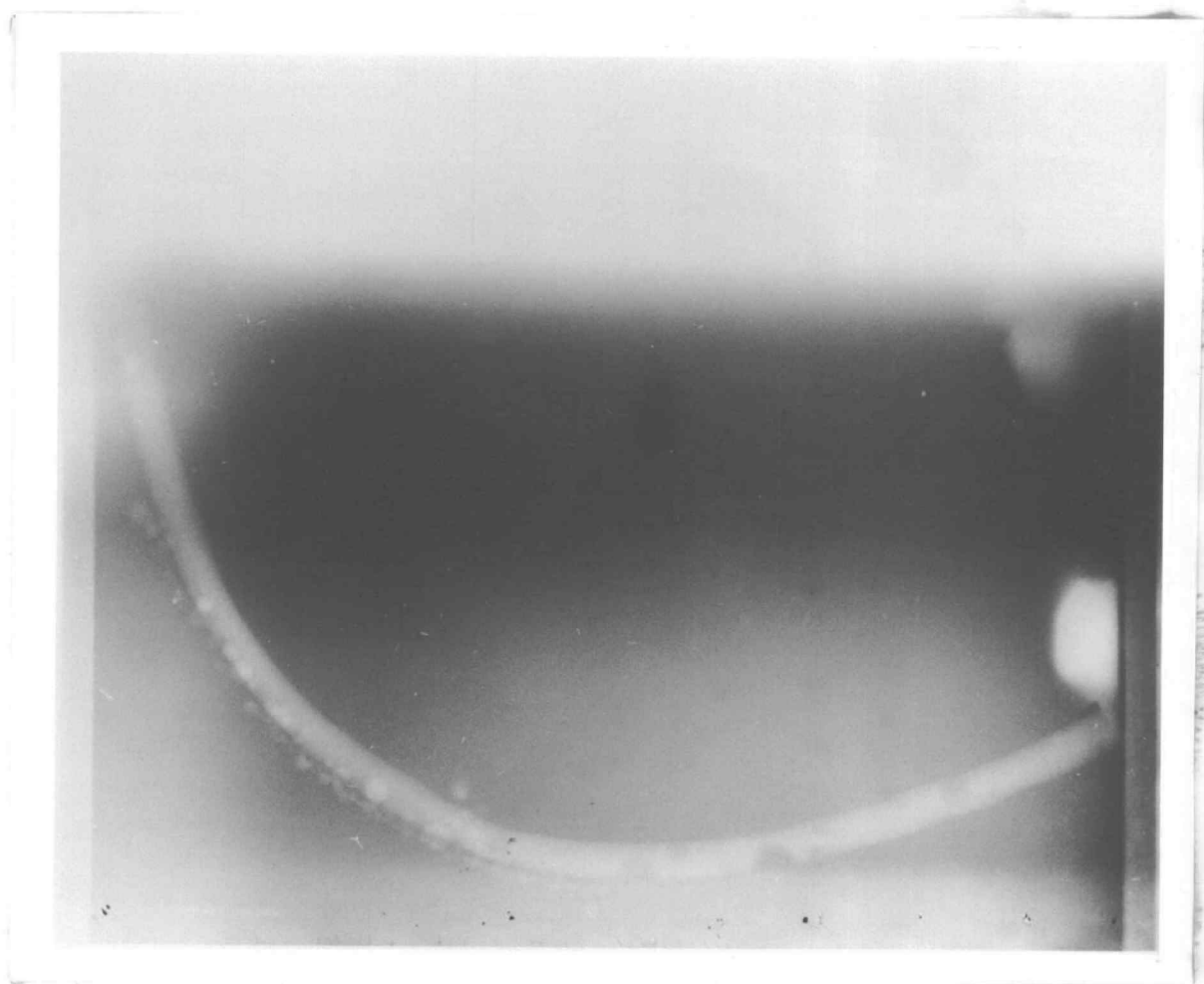


Figure 6.5 Integrated Flux Pulsed Radiography  
H<sub>2</sub>O with Air Bubbles in Thin Box  
Peak Power: 3,060 MW

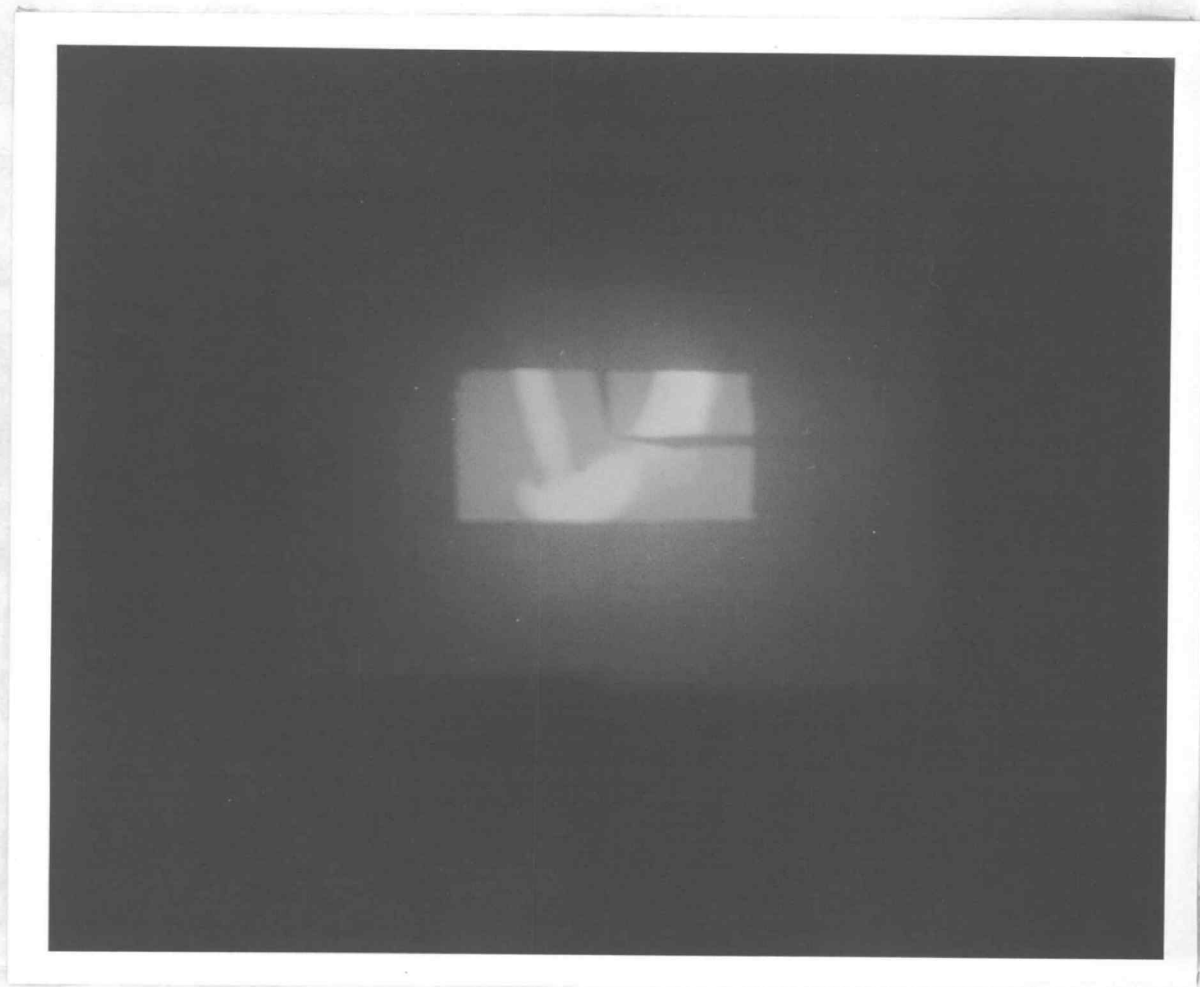


Figure 6.6 Integrated Flux Pulsed Radiography  
H<sub>2</sub>O with Air Bubbles in Thin Box  
Peak Power: 3,060 MW



Figure 6.7 Integrated Flux Pulsed Radiography  
H<sub>2</sub>O with Air Bubbles in Thin Box  
Peak Power: 3,040 MW



Figure 6.8    Integrated Flux Pulsed Radiography  
H<sub>2</sub>O Boiling in Thin Box  
( Beginning of Boiling )  
Peak Power: 3,040 MW

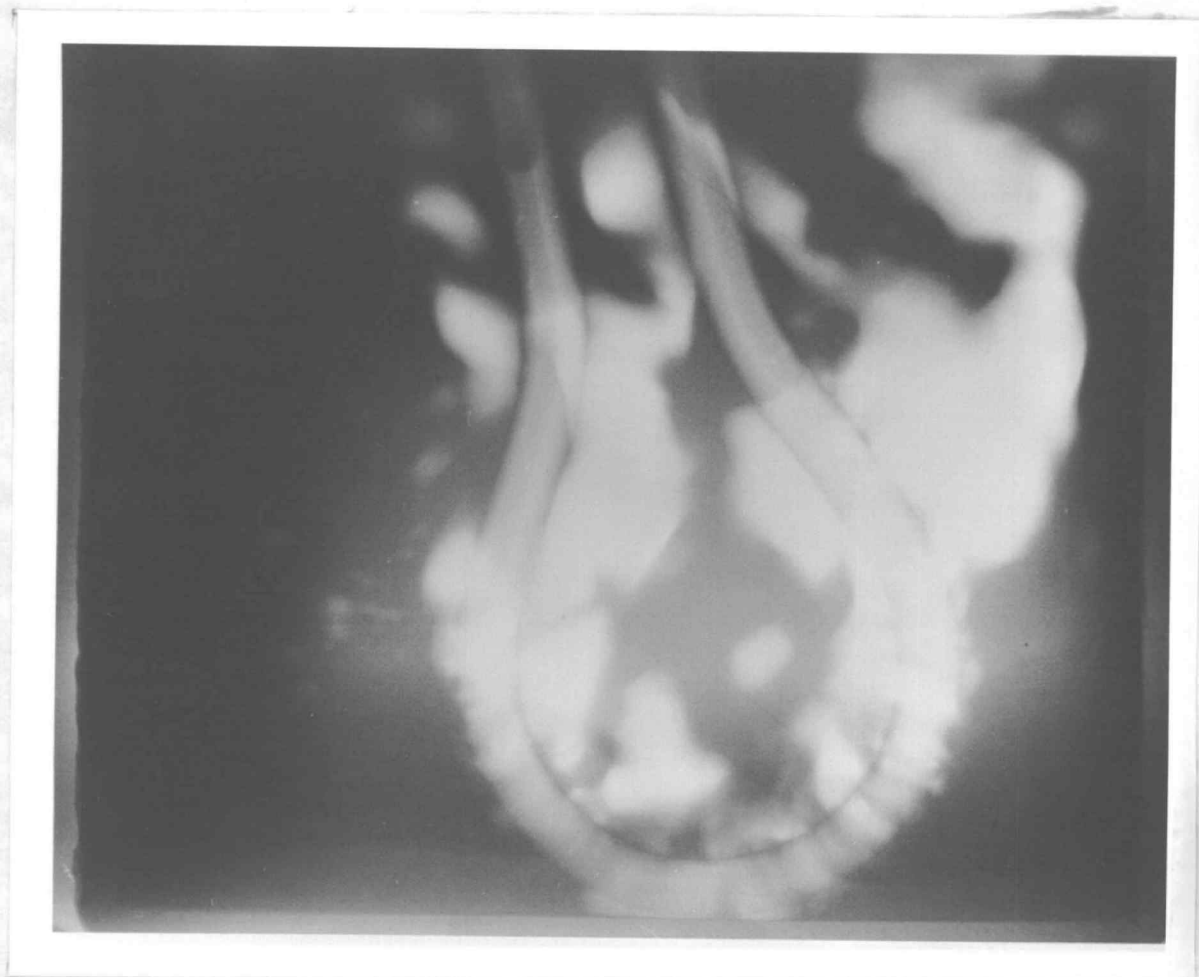


Figure 6.9 Integrated Flux Pulsed Radiography  
H<sub>2</sub>O Boiling in Thin Box  
Peak Power: 3,060 MW

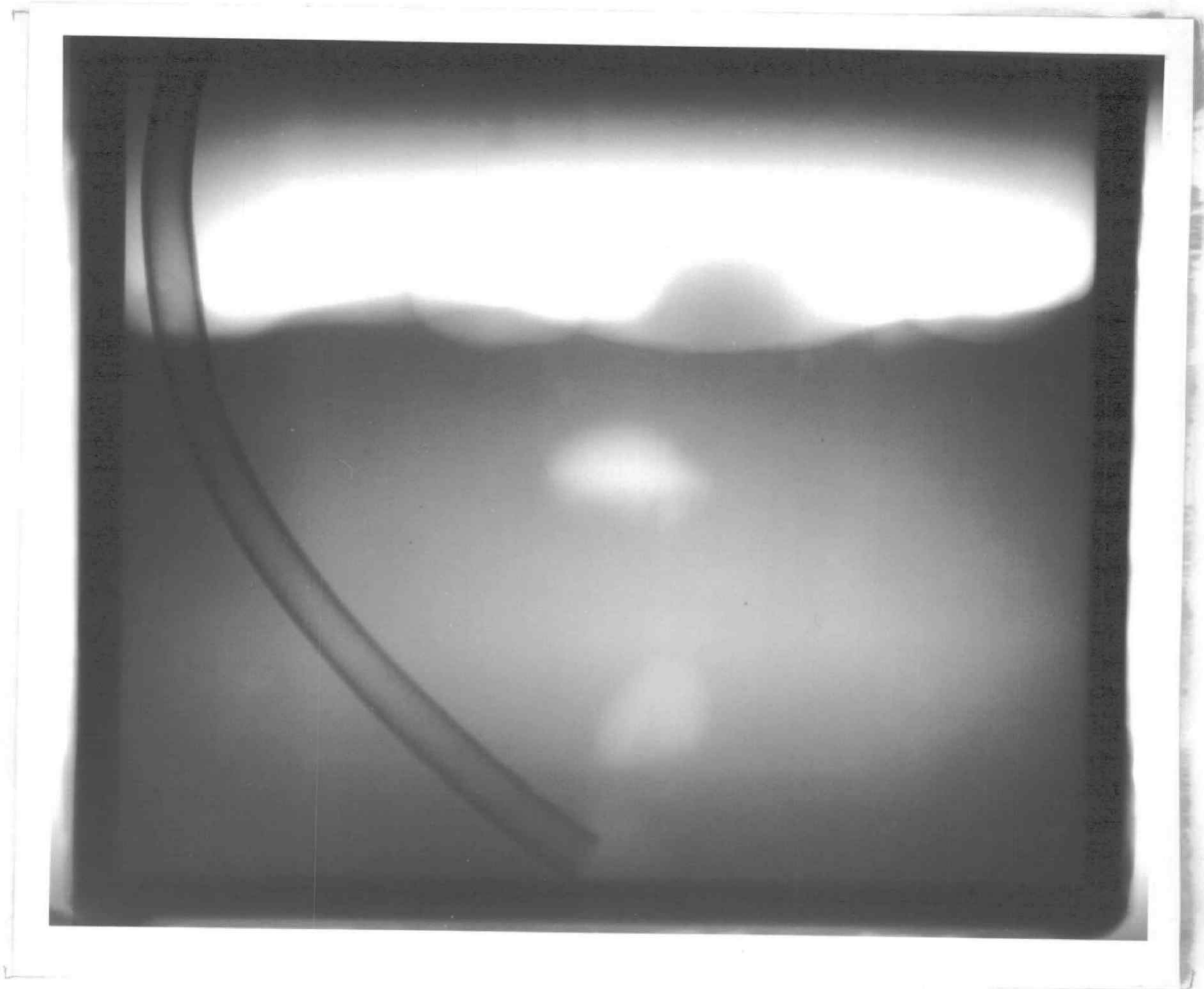


Figure 6.10 Integrated Flux Pulsed Radiography  
D<sub>2</sub>O with Air Bubbles in Thick Box  
Peak Power: 3,040 MW

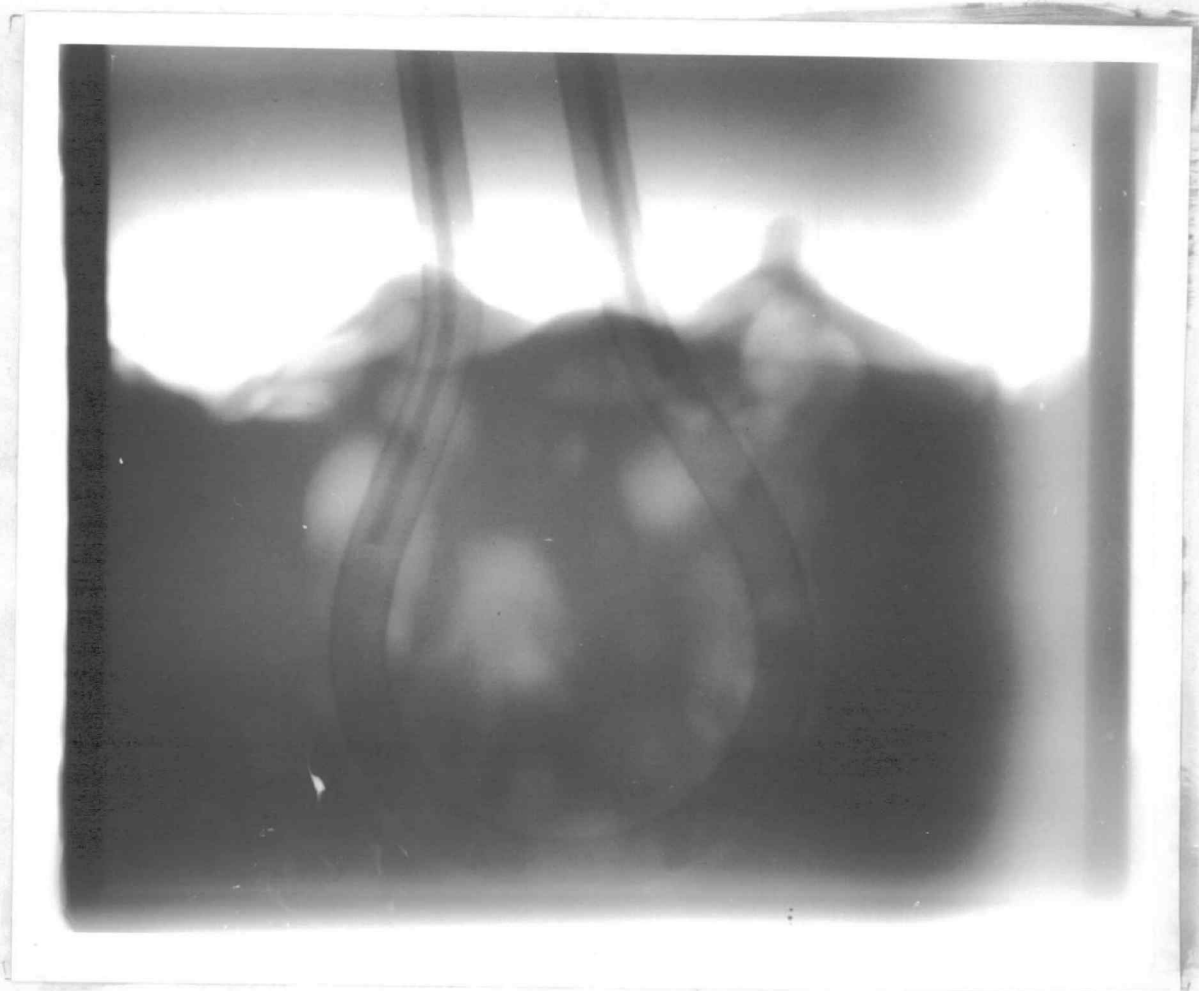


Figure 6.11 Integrated Flux Pulsed Radiography  
D<sub>2</sub>O Boiling in Thick Box  
Peak Power: 3,000 MW

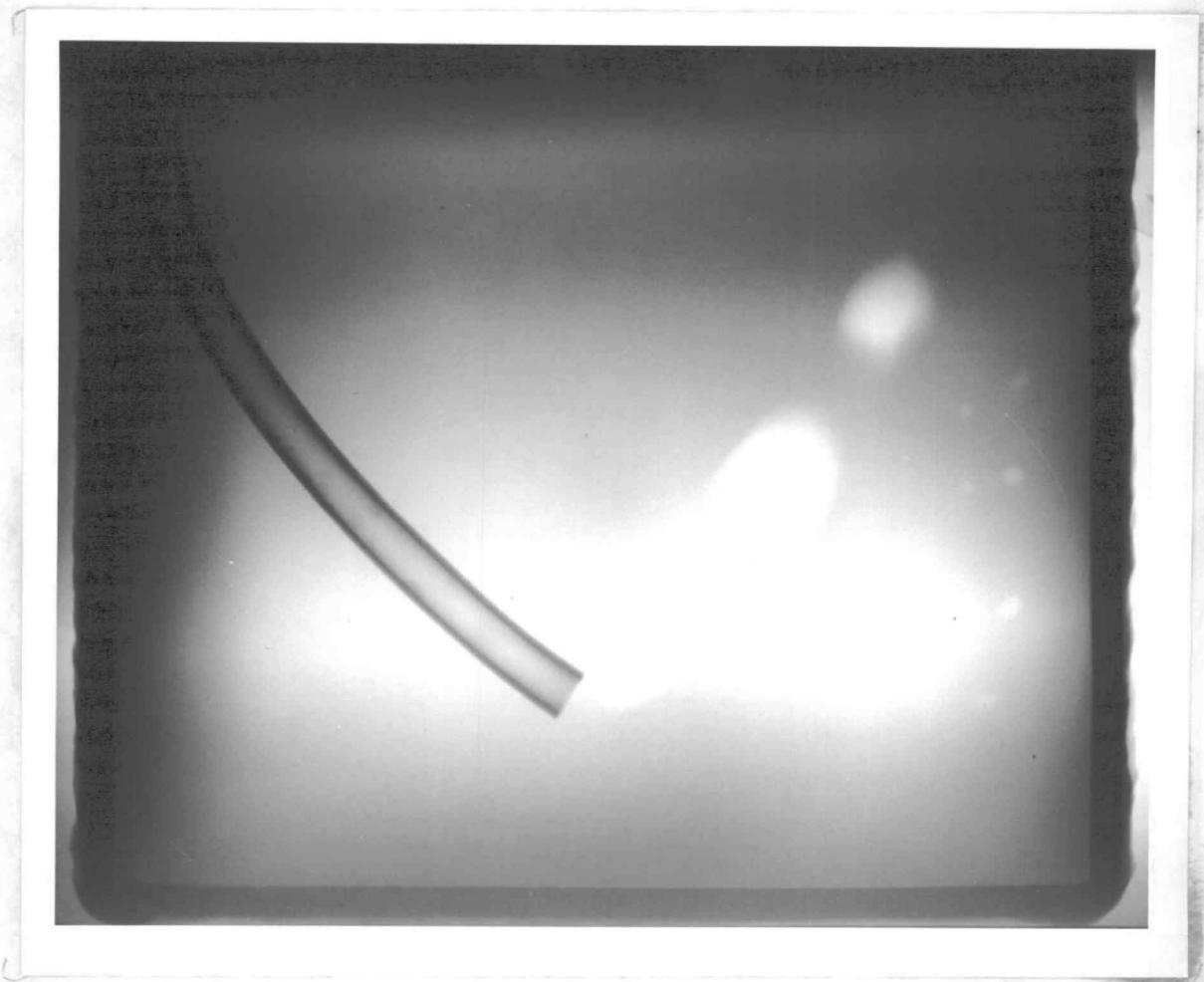


Figure 6.12 Integrated Flux Pulsed Radiography  
D<sub>2</sub>O with Air Bubbles in Thin Box  
Peak Power: 3,020 MW

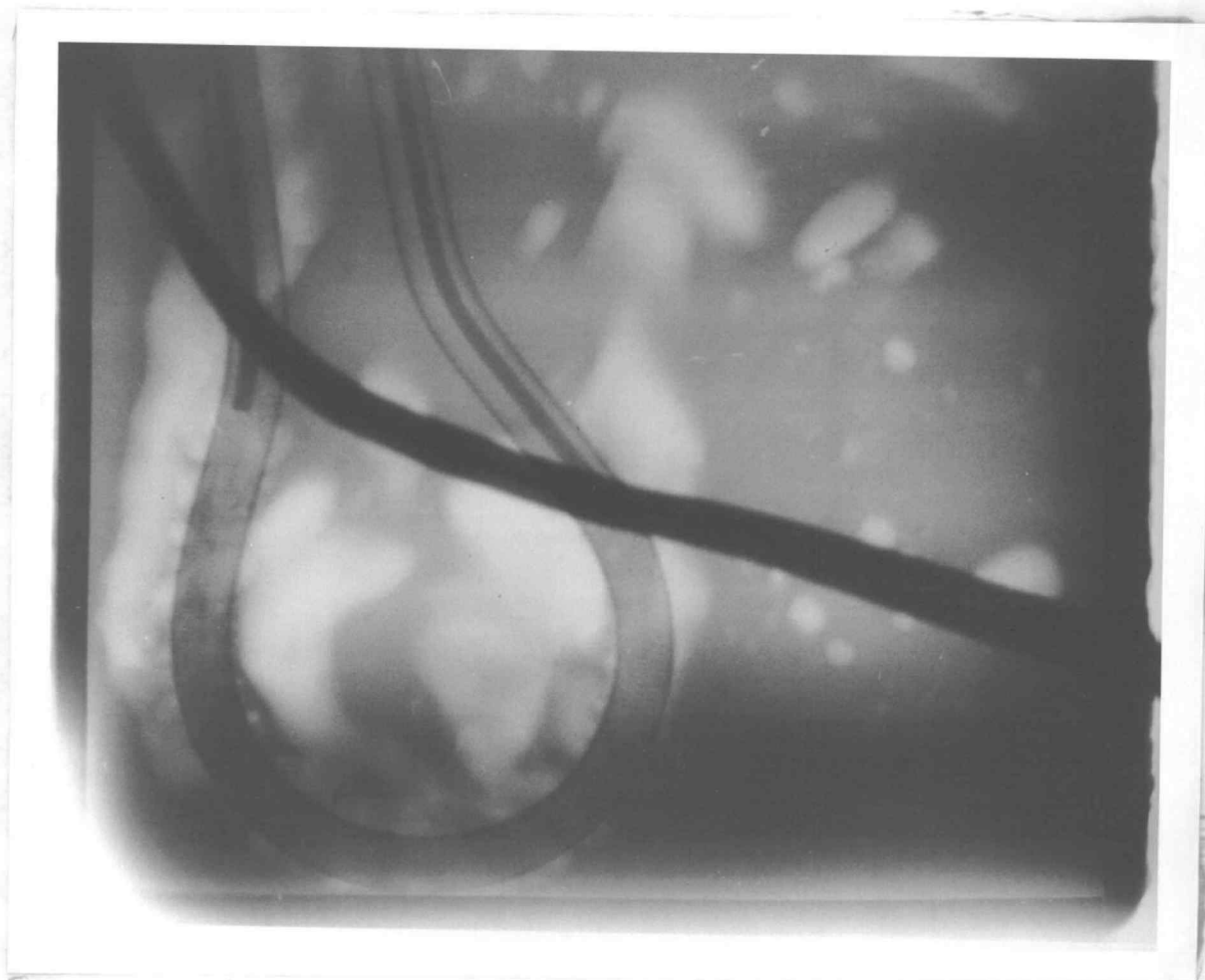


Figure 6.13 Integrated Flux Pulsed Radiography  
D<sub>2</sub>O Boiling in Thin Box  
Peak Power: 3,000 MW

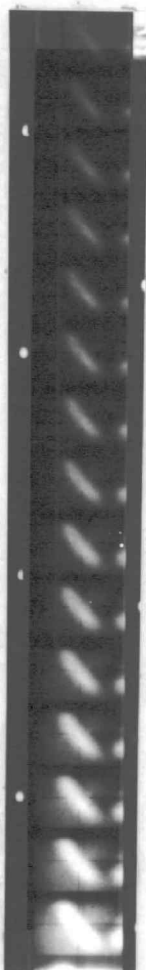


Figure 6.14  
Water with Air  
Bubbles in Thin  
Box  
Frame Rate:  
5,000 fs/s  
F-stop: 1.2  
Peak Power:  
3,080 MW

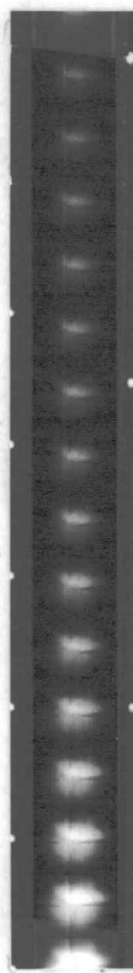


Figure 6.15  
Boiling Water  
in Thin Box  
Frame Rate:  
1,000 fs/s  
F-stop: 1.2  
Peak Power:  
3,160 MW

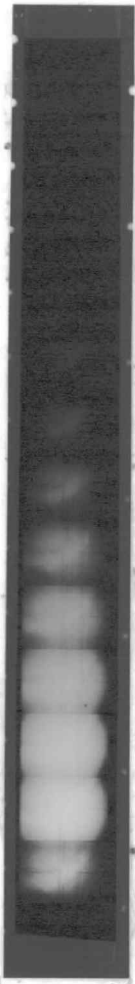


Figure 6.16  
Boiling Water  
in Thin Box  
Frame Rate:  
1,000 fs/s  
F-stop: 2.0  
Peak Power:  
3,140 MW



Figure 6.17  
Boiling Water  
in Thin Box  
Frame Rate:  
500 fs/s  
F-stop: 4.0  
Peak Power:  
3,120 MW

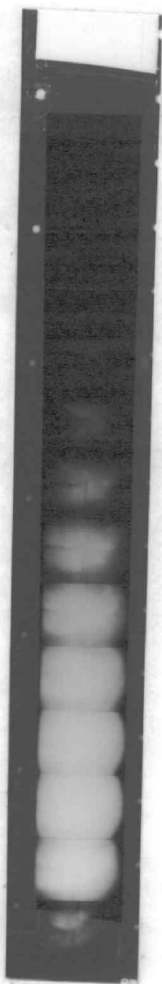


Figure 6.18  
Boiling Water  
in Thin Box  
Frame Rate:  
250 fs/s  
F-stop: 1.2  
Peak Power:  
187 MW

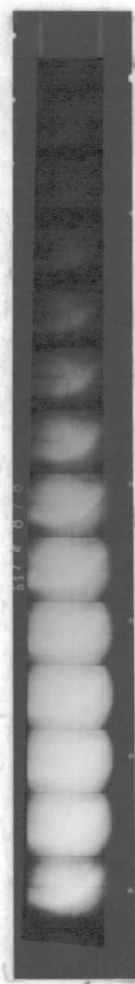


Figure 6.19  
Boiling Water  
in Thin Box  
Frame Rate:  
125 fs/s  
F-stop: 1.2  
Peak Power:  
116 MW

is rather uniform due to lower peak power and slower frame rate set.

In order to make comparisons, photographs were taken with an ordinary camera at different speed. These are shown in figure 6.20 through figure 6.23. The purpose of these pictures is two-fold, first, they were used to determine the speeds required of the neutron radiography system; secondly, they help significantly in the interpretation of the neutron radiographs. Figure 6.20 and figure 6.21 are the photographs with a camera speed of  $1/1000$  sec (i.e., exposure time of 1 msec) of the water with air bubbles and boiling water. These photographs would correspond to the radiographs taken by high speed camera with frame rate of 400 frames/sec. Figure 6.22 and figure 6.23 are the photographs with camera speed of  $1/125$  sec (i.e., exposure time of 8 msec) of the two-phase flow. These photographs correspond to the integrated flux pulsed radiographs with an "exposure time" of 8 msec; which approximately equals the FWHM of pulse peak power from 1500 MW to 3000 MW.

The visibility of a bubble with various diameters in water (or heavy water) with various thicknesses can be predicted by either the  $S_N$  approximation or the Monte Carlo method. The applicability of these computer models can be estimated by comparing the expected visibilities with those measured by a densitometer which can show the different film densities of the images of the bubbles in water (or heavy water) on the film. The expected and measured visibilities are given in table 6.1, where  $W$  is the thickness of the box and  $D$  is the diameter of the bubble. The visibility is expressed in terms of the relative exposure density of the images of the bubble and

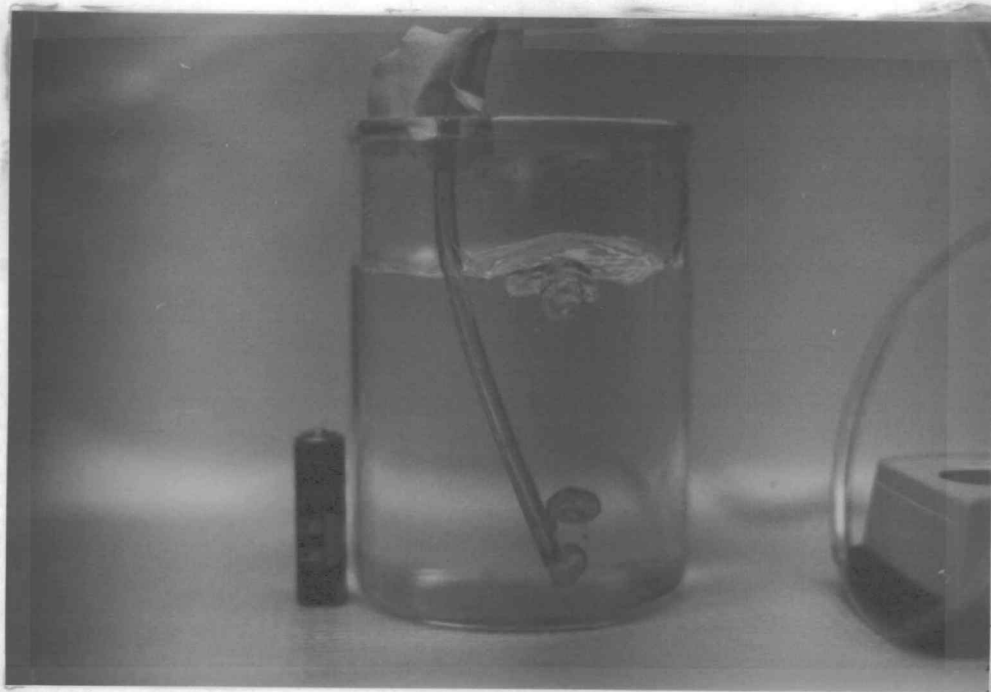


Figure 6.20 Water with Air Bubbles with Exposure Time of 1 ms

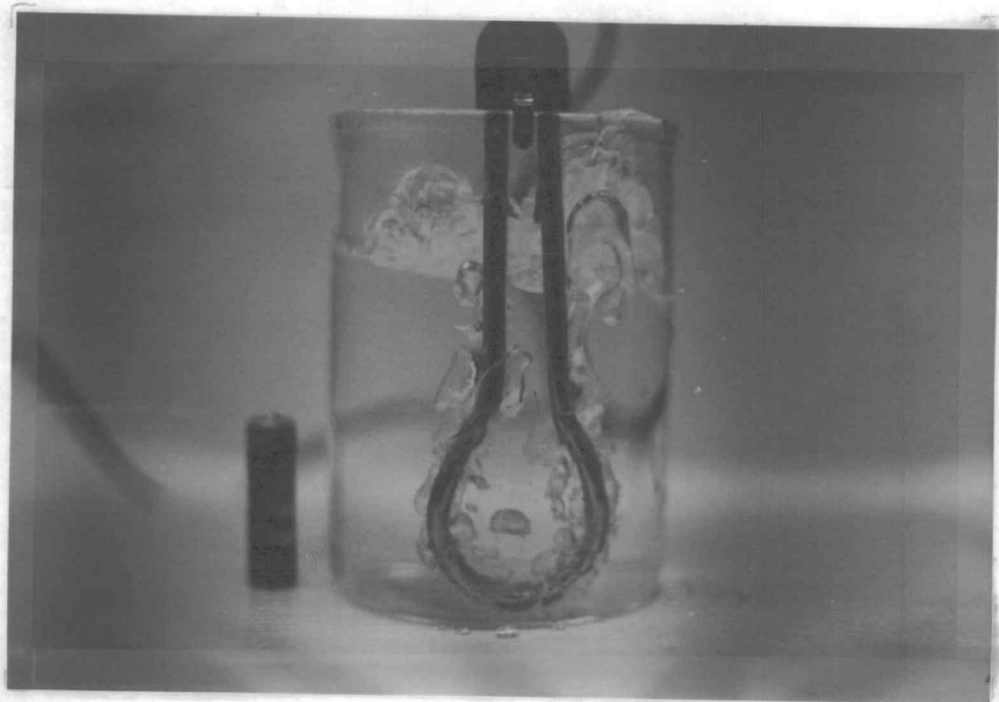


Figure 6.21 Boiling Water with Exposure Time of 1 ms

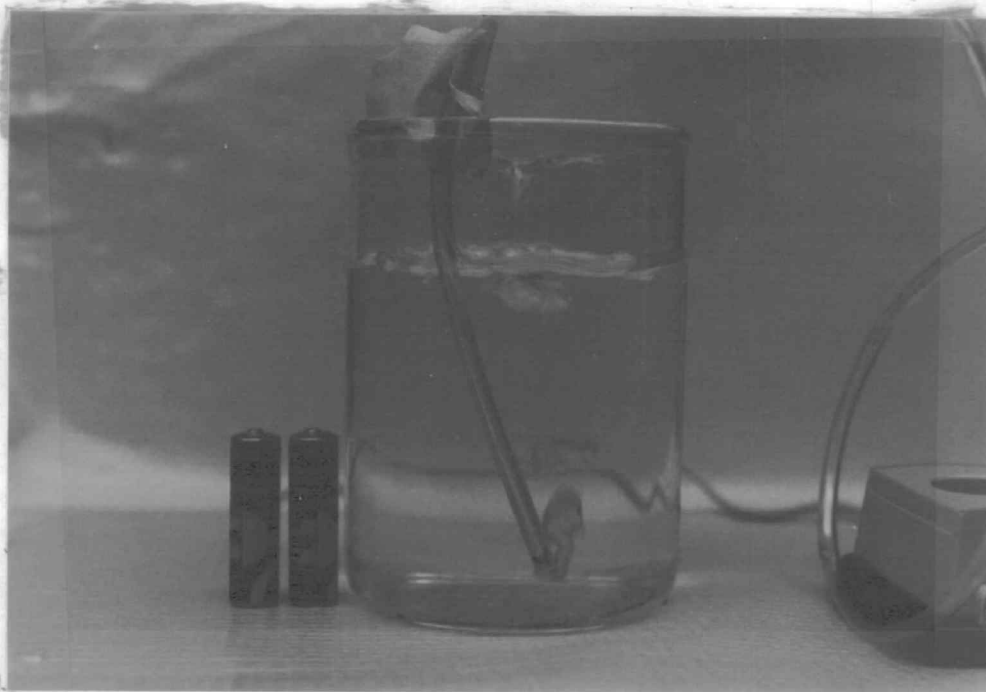


Figure 6.22 Water with Air Bubbles with Exposure Time of 8 ms

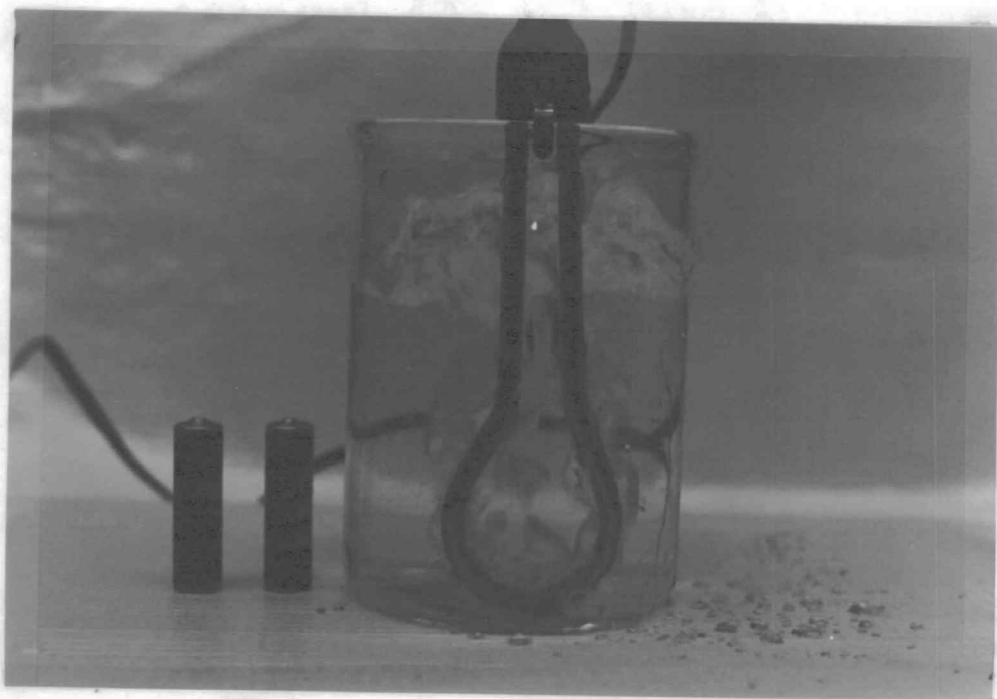


Figure 6.23 Boiling Water with Exposure Time of 8 ms

fluid, i.e.,  $I_{\text{bubble}}/I_{\text{fluid}}$ . The effect of using an anti-scatter grid is also shown in table 6.1 and it is obvious that the visibilities would be improved significantly by the anti-scatter grid. In table 6.1 if  $I_{\text{bubble}}/I_{\text{fluid}}$  is equal or very close to 1, that means the bubble is "invisible", on the other hand, if  $I_{\text{bubble}}/I_{\text{fluid}}$  is very larger than 1, that means the bubble is "visible". For example, a bubble with 0.2 cm diameter in the thick box is invisible while it is visible in the thin box.

The expected visibilities of a 0.5 cm diameter bubble in various thickness of light water and heavy water are plotted in figure 6.24 through figure 6.27. In these figures, if the relative visibilities are close to the broken line, that means the bubble is getting more and more invisible.

## 6.2 Conclusions

The work on the neutron radiography system has resulted in successful achievement of the initial goal of radiographing the simulated two-phase flow. The study of the system has also brought to light some interesting aspects in the radiographing of the real two-phase flow in reactor channels.

1. The visibility of the bubble is atrongly depedent on the thickness of the water. Two-phase flow can be visible with the thickness of water under 2 cm. If an anti-scatter grid is used, this can be increased up to 4 cm.
2. If heavy water is used instead of light water, two-phase flow can be seen through 4 cm. If an anti-scatter grid is used, this can be increased up to 6 cm.

Table 6.1 Expected and Measured Visibilities  
of a Bubble in Light and Heavy Water

			Expected by Computer Codes		Measured by Densitometer
W (cm)	D (cm)	Fluid	$S_N$ Approximation $I_{\text{bubble}}/I_{\text{fluid}}$	Monte Carlo Method $I_{\text{bubble}}/I_{\text{fluid}}$	$I_{\text{bubble}}/I_{\text{fluid}}$
3.2	0.2	H <sub>2</sub> O	1.06 (1.06) *	1.09 (1.18)	~1.0
		D <sub>2</sub> O	1.12 (1.16)	1.15 (1.23)	N/A
	0.5	H <sub>2</sub> O	1.18 (1.19)	1.10 (1.24)	N/A
		D <sub>2</sub> O	1.14 (1.17)	1.21 (1.29)	~1.2
	1.0	H <sub>2</sub> O	1.40 (1.41)	1.28 (1.30)	N/A
		D <sub>2</sub> O	1.20 (1.43)	1.25 (1.40)	~1.3
0.8	0.2	H <sub>2</sub> O	1.14 (1.50)	1.24 (1.50)	~1.2
		D <sub>2</sub> O	1.00 (1.08)	1.19 (1.36)	~1.1
	0.5	H <sub>2</sub> O	1.45 (3.43)	1.26 (1.78)	~1.9
		D <sub>2</sub> O	1.20 (1.24)	1.21 (1.44)	~1.2
	0.7	H <sub>2</sub> O	1.65 (7.34)	1.36 (1.43)	~2.5
		D <sub>2</sub> O	1.30 (1.38)	1.25 (1.31)	~1.5

\* Values in parentheses are with anti-scatter grid.

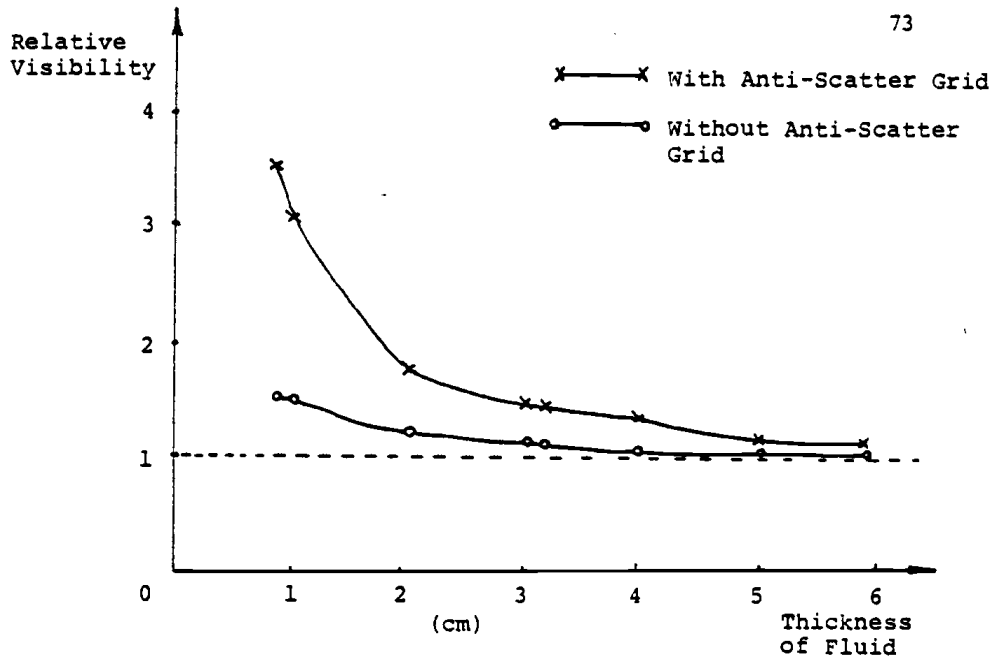


Figure 6.24 Expected Visibility of a 0.5 cm-Diameter Bubble vs. Thickness of H<sub>2</sub>O Calculated by S<sub>N</sub> Approximation

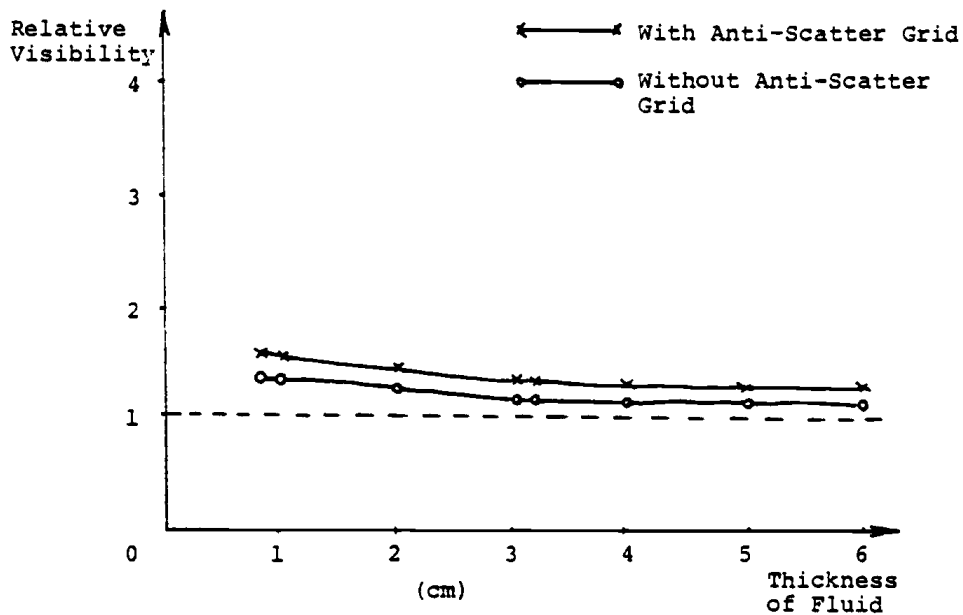


Figure 6.25 Expected Visibility of a 0.5 cm-Diameter Bubble vs. Thickness of D<sub>2</sub>O Calculated by S<sub>N</sub> Approximation

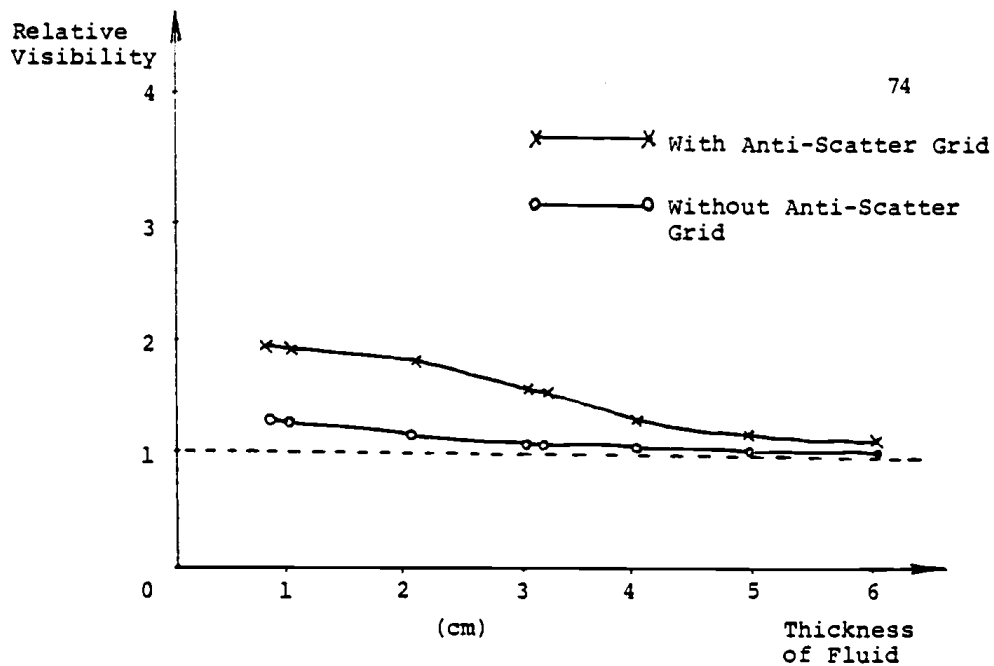


Figure 6.26 Expected Visibility of a 0.5 cm-Diameter Bubble vs. Thickness of H<sub>2</sub>O Calculated by Monte Carlo Method

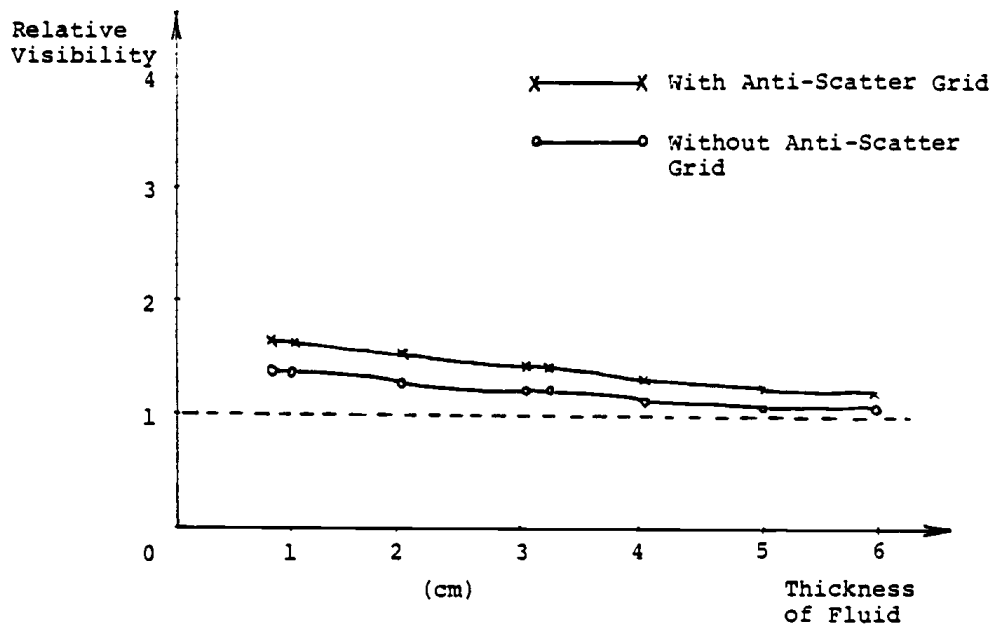


Figure 6.27 Expected Visibility of a 0.5 cm-Diameter Bubble vs. Thickness of D<sub>2</sub>O Calculated by Monte Carlo Method

3. The anti-scatter grid can improve the visibility of the two-phase flow only at the expense of losing the imaging sharpness due to increasing the distance between the object and imaging device.
4. If the thickness of the fluids is under 1 cm, the image of two-phase flow in light water is clearer than that in heavy water due to the larger difference of macroscopic cross-sections between light water and air bubbles.
5. The images of the two-phase flow can be frozen in the high speed motion radiography by camera while some blurring occurred in the integrated flux pulsed radiography.
6. To get a more uniformly distributed exposure on each frame of the high speed motion radiography, pulses with low peak power(  $\sim 100$  MW) should be combined with a slow camera frame rate(  $\sim 125$  frames/sec).

## VII. BIBLIOGRAPHY AND APPENDICES

1. H. Berger, Neutron Radiography, Elsevier, New York, 1965.
2. J. Walker, "Radiography With Neutrons", Radiography With Neutrons, Conference at the University of Birmingham, September, 1973.
3. J. P. Barton, Appl. Mats. Res., 4(1965)90.
4. G. Bell, S. Glasstone, Nuclear Reactor Theory, USAEC, 1971, p. 319.
5. D. A. Tollefson, "Application of High Speed Motion Neutron Radiography Techniques to Liquid Streams Injected into Steel Pressure Chambers", M.S. Thesis, Oregon State University, 1980.
6. D. J. Hughes, R. B. Schwartz, Neutron Cross Sections, USAEC, 1962.
7. J. C. Ringle, T. V. Anderson, A. G. Johnson, Safety Analysis Report for the Oregon State University TRIGA Reactor, August, 1968.
8. "Beam Port #3 Facility Description, Access Control and Operational Safety Procedures", Oregon State University, 1979.
9. J. Lamarsh, Introduction to Nuclear Engineering, Addison-Wesley, 1975, p. 83.
10. D. L. Hetrick, Dynamics of Nuclear Reactors, 1971, p. 164.
11. A. H. Robinson, J. P. Barton, "High Speed Motion Neutron Radiography", Transactions American Nuclear Society, Vol. 15, 1972, p. 140.
12. R. H. Bossi, "Neutron Radiography", Ph.D. Thesis, Oregon State University, 1976.
13. J. R. Raw, W. L. Parker, "Measurement of Anti-Scatter Grid Effectiveness in Thermal Neutron Radiography of Hydrogenous Materials", Nuclear Technology, Vol. 16, 1972, p. 458.

14. J. D. Duderstadt, L. J. Hamilton, Nuclear Reactor Analysis, John Wiley & Sons, 1976, p. 128.
15. R. H. Bossi, "Neutron Radiography", Ph.D. Thesis, Oregon State University, 1976.
16. J. R. Lamarsh, Nuclear Reactor Theory, 1966, p. 53.

## APPENDIX I

```

*****
*   LANCELOT WANG      APRIL 20, 80 *
*THIS PROGRAM USES SN APPROXIMATION*
* OF NEUTRON FLUX SCATTERED IN THE *
* WATER WITH OR WITHOUT A BUBBLE   *
* THE RATIO OF THIS VALUE CAN BE   *
* USED TO PREDICT THE SHARPNESS OF *
* THE BUBBLE ON THE FILM           *
* ALSO THE EFFECT OF USING ANTI-   *
* SCATTER GRID IS ESTIMATED        *
*****

```

```

PROGRAM SNCODE(INPUT,OUTPUT)
DIMENSION WGT(20),U(20),Q(500),FLUX(500,20)
DIMENSION X(500),FWGT(500),QOLD(500)
DIMENSION C(500),CPOS(500),CNEG(500)
999 PRINT*,"INPUT THE THICKNESS OF THE WATER; W(CM)"
PRINT*,"THE THICKNESS OF THE BUBBLE; D(CM)"
PRINT*,"AND NO. OF INTERVALS OF THE WATER; INT"
READ*,W,D,INT
PRINT*,"INPUT THE MACROSCOPIC X'SECTIONS OF WATER AND AIR"
PRINT*,"SIGMAW AND SIGMAA"
READ*,SIGMAW,SIGMAA
PRINT*,"INPUT ORDER OF SN; N"
READ*,N
IF(N.EQ.10)GO TO 77
PRINT*,"INPUT WEIGHTS; WGT(I) AND ROOTS; U(I)"
PRINT*,"OF THE GAUSSIAN INTEGRATION"
READ*,(WGT(I),U(I),I=1,N)
GO TO 88
77 WGT(1)=.06667
WGT(2)=.14945
WGT(3)=.21909
WGT(4)=.26927
WGT(5)=.29552
WGT(6)=WGT(5)
WGT(7)=WGT(4)
WGT(8)=WGT(3)
WGT(9)=WGT(2)
WGT(10)=WGT(1)
U(1)=-.97391

```

```

U(2)=-.86506
U(3)=-.67941
U(4)=-.43340
U(5)=-.14887
U(6)=-U(5)
U(7)=-U(4)
U(8)=-U(3)
U(9)=-U(2)
U(10)=-U(1)
88 RINT=INT
H=W/RINT
INTL=.5*(W-D)/H+1
INTR=(W-.5*(W-D))/H
PRINT*, " "
IF(D.EQ.0.)GO TO 1
PRINT*, "*****THE CASE FOR A BUBBLE IN THE WATER*****"
GO TO 2
1 PRINT*, "*****THE CASE FOR WATER WITHOUT BUBBLE*****"
2 INTP=INT+1
C*****INITIALIZE FLUX AND Q
DO 10 I=1,INTP
Q(I)=0.
DO 10 J=1,N
FLUX(I,J)=0.
10 CONTINUE
C*****GIVEN THE INCIDENT FLUX
FLUX(1,N)=1.0
DO 20 I=1,INTP
X(I)=H*(I-1)
20 CONTINUE
C*****START THE OUTER ITERATION ON Q
IQ=0
100 IQ=IQ+1
IF(IQ.GT.200)GO TO 200
C*****CALCULATE THE TOTAL FLUX
DO 30 K=1,INTP
SUM1=0.
DO 31 J=1,N
SUM1=SUM1+FLUX(K,J)*WGT(J)
31 CONTINUE
FWGT(K)=SUM1
30 CONTINUE
DO 40 I=1,INTP
QOLD(I)=Q(I)
40 CONTINUE
DO 50 K=1,INT

```

C

```

SUM=FWGT(K)+FWGT(K+1)
IF(K.GT.INTL.AND.K.LT.INTR)GO TO 41

Q(K)=SIGMAW*H*SUM/4.
GO TO 50
41 Q(K)=SIGMAA*H*SUM/4.
50 CONTINUE
DO 60 I=1,INT
TEST=ABS((Q(I)-QOLD(I))/Q(I))
IF(TEST.GE..0001)GO TO 61
60 CONTINUE
GO TO 300
61 DO 70 J=1,N
IF(U(J).GT.0.)GO TO 71
DO 72 K=1,INT
L=INT+1-K
IF(L.LT.INTR.AND.L.GT.INTL)GO TO 722
WANG=SIGMAW*H/(2.*U(J))
GO TO 723
722 WANG=SIGMAA*H/(2.*U(J))
723 FLUX(L,J)=FLUX(L+1,J)*(1.0+WANG)/(1.0-WANG)
1-Q(L)/(U(J)*(1.0-WANG))
72 CONTINUE
GO TO 70
71 DO 73 K=2,INTP
IF(K.GT.INTL.AND.K.LT.INTR)GO TO 711
WANG=SIGMAW*H/(2.*U(J))
GO TO 712
711 WANG=SIGMAA*H/(2.*U(J))
712 FLUX(K,J)=FLUX(K-1,J)*(1.0-WANG)/(1.0+WANG)
1+Q(K-1)/(U(J)*(1.0+WANG))
73 CONTINUE
70 CONTINUE
GO TO 100
200 PRINT*,"THE ITERATIONS ON Q IS OVER 200"
C*****CALCULATE THE CURRENTS
300 DO 301 K=1,INTP
SUM1=0.
SUM2=0.
DO 302 J=1,N
IF(U(J).GT.0.)GO TO 303
SUM1=SUM1+U(J)*FLUX(K,J)*WGT(J)
GO TO 302
303 SUM2=SUM2+U(J)*FLUX(K,J)*WGT(J)
302 CONTINUE
C(K)=SUM1+SUM2

```

```

      CNEG(K)=SUM1
      CPOS(K)=SUM2
301  CONTINUE
      PRINT*, " "
      PRINT*, "NO. OF ITERATION ON Q = ", IQ
      PRINT*, " "
      PRINT*, "      MESH      X(I)      TOTAL      NET      J+      J-"
      PRINT*, "      POINT      (CM)      FLUX      CURRENT"
      PRINT 1000, (K, X(K), FWGT(K), C(K), CPOS(K), CNEG(K), K=1, INTP)
1000  FORMAT(1X, I7, 5F8.5)
      PRINT*, " "
      PRINT*, "      ANGLE      WEIGH      U"
      PRINT 1001, (I, WGT(I), U(I), I=1, N)
1001  FORMAT(2X, I8, 2F10.6)
      PRINT*, " "
      PRINT 1003, (I, I=1, N)
1003  FORMAT("      MESH ANGLE      ", 10(5X, I2))
      DO 1004 K=1, INTP
      PRINT 1005, (K, (FLUX(K, J), J=1, N))
1005  FORMAT(2X, I4, 8X, 10F7.5)
1004  CONTINUE
      PRINT*, " "
      PRINT*, "DO YOU WANT ANOTHER RUN ?"
      READ 666, IANS
666  FORMAT(A3)
      IF(IANS.EQ.3HYES) GO TO 999
      STOP
      END

```

## APPENDIX II

C  
C  
C  
C  
C  
C  
C  
C  
C  
C  
C  
C

```

*****
*      LANCELOT WANG          APRIL 16, 1980      *
* MONTE CARLO CODE FOR PREDICTING THE NEUTRON    *
* BEAM INTENSITY DISTRIBUTION AFTER SCATTERED    *
* BY WATER OF VARIOUS THICKNESS WITH A BUBBLE    *
* OF VARIOUS SIZE INSIDE AND PREDICTING THE      *
* EFFECTS OF USING AN ANTI-SCATTERING GRID      *
*****

```

```

PROGRAM MONTE(INPUT,OUTPUT,TAPE6=OUTPUT)
DIMENSION NHIST(500),NOUT(500),NGRID(500),YOUT(500)
999 PRINT*,"INPUT THE SIZE OF THE BOX; W(CM)*H(CM)"
PRINT*,"AND THE DIAMETER OF THE BUBBLE; D"
READ*,W,H,D
PRINT*,"INPUT THE HEIGHT THAT THE INCOMING NEUTRON"
PRINT*,"BEAMS COVER; YHEIG"
READ*,YHEIG
PRINT*,"INPUT THE NUMBER OF THE DISCRETIZED NEUTRON"
PRINT*,"BUNDLES; NBUND"
READ*,NBUND
NBUNDP=NBUND+1
PRINT*,"INPUT NBUND+1 VALUES OF NEUTRON HISTORIES"
PRINT*,"IN EACH BUNDLE; NHIST(I), WHICH CAN BE"
PRINT*,"CONSTANT OR VARIABLES DEPENDING ON THE"
PRINT*,"INCOMING NEUTRON BEAM INTENSITY"
READ*,(NHIST(I),I=1,NBUNDP)
PRINT*,"INPUT MACROSCOPIC 'SECTION OF WATER(OR D2O); SIGMAT"
READ*,SIGMAT
PRINT*,"INPUT AVERAGE COSINE OF WATER(OR D2O);U"
READ*,U
PRINT*,"DO YOU WANT TO USE ANTI-SCATTERING GRID ?"
PRINT*,"IF YES, INPUT RATIO OF L/D OF THE GRID; RGRID"
PRINT*,"IF NO, INPUT 0."
READ*,RGRID
RGRID=RGRID/((RGRID**2.+1.)**.5)
DIV=YHEIG/(NBUND+0.)
PI=3.141592654
DELTA=.1*D/2.
RANGE=YHEIG/2.+YHEIG/(2.*NBUND)
DO 50 I=1,NBUNDP

```

```

      NOUT(I)=0
      NGRID(I)=0
50  CONTINUE
C*****STARTING NEUTRON HISTORY IN THE LEFT SIDE OF THE WATER
      DO 100 I=1,NBUNDP
      NHISTI=NHIST(I)
      DO 200 II=1,NHISTI
C*****INITIALIZE THE INITIAL POSITION OF NEUTRON HISTORY
      UOLD=1.
      P=(-1./SIGMAT)*ALOG(RANF(RN))
      X=-W/2.+P
      Y=-YHEIG/2.+DIV*(I-1)
C*****ASSUME THE SCATTERING COSINE IS U IN EVERY COLLOSION
      ANG=ACOS(U)
203  PHI=2.*PI*RANF(RN)
      UNEW=UOLD*U+(1.-UOLD**2.)**.5*SIN(ANG)*COS(PHI)
      SIGN=RANF(RN)
      IF(SIGN.LT..5)GO TO 1
      AN=ACOS(UNEW)
      GO TO 2
1  AN=-ACOS(UNEW)
2  C=UNEW
      S=SIN(AN)
      P=(-1./SIGMAT)*ALOG(RANF(RN))
      X=X+P*C
      Y=Y+P*S
C*****TEST IF THE NEUTRON IS SCATTERED OUT OF THE LEFT BOUNDARY
301 IF(X.LE.(-W/2.))GO TO 200
C*****TEST IF THE NEUTRON IS SCATTERED OUT OF THE UPPER
C*****OR LOWER BOUNDARY
      IF(ABS(Y).GT.(H/2.))GO TO 200
C*****TEST IF THE NEUTRON IS ENTERING THE BUBBLE REGION
      RAD=SQRT(X**2.+Y**2.)
      IF(RAD.LE.(D/2.))GO TO 300
      UOLD=UNEW
C*****TEST IF THE NEUTRON IS LEAVING THE RIGHT SIDE BOUNDARY
      IF(X.GT.(W/2.))GO TO 400
      GO TO 203
C*****ENTERING THE BUBBLE REGION
C*****THE NEUTRON GOES IN A STRAIGHT WAY WITHOUT SCATTERING
300 X=X+DELTA*C
      Y=Y+DELTA*S
      GO TO 301
C*****COLLECTING NEUTRONS ON THE RIGHT SIDE BOUNDARY
400 Y=Y-(X-W/2.)*TAN(AN)
      IF(ABS(Y).GT.RANGE)GO TO 200

```

```

      NY=(Y+RANGE)/DIV+1
      NOUT(NY)=NOUT(NY)+1
      IF(RGRID.EQ.0.)GO TO 200
C*****TEST IF THE NEUTRON IS COLLIMATED BY THE GRID
      IF(C.LE.RGRID)GO TO 200
      NGRID(NY)=NGRID(NY)+1
200  CONTINUE
100  CONTINUE
      PRINT*, " "
      PRINT*, "          INCOMING      OUTGOING      NEUTRONS"
      PRINT*, "          NEUTRON      NEUTRON      MODULATED"
      PRINT*, "          INTENSITY    INTENSITY    BY GRID"
      PRINT*, " "
      DO 1000 I=1,NBUNDP
      YOUT(I)=-YHEIG/2.+DIV*(I-1)
      IF(ABS(YOUT(I)).LE.(D/2.))GO TO 2001
      WRITE(6,2000)YOUT(I),NHIST(I),NOUT(I),NGRID(I)
2000  FORMAT("Y= ",F5.2,3I12)
      GO TO 1000
2001  WRITE(6,2002)YOUT(I),NHIST(I),NOUT(I),NGRID(I)
2002  FORMAT("Y= ",F5.2,"BUBBLE",3I12)
1000  CONTINUE
      PRINT*, " "
      PRINT*, "DO YOU WANT ANOTHER RUN ?"
      READ 33, IANS
33  FORMAT(A3)
      IF(IANS.EQ.3HYES)GO TO 999
      STOP
      END

```